Available online at www.sciencedirect.com
ScienceDirect
Sensors and Actuators A 135 (2007) 713–730
SENSORS AND ACTUATORS A PHYSICAL
www.elsevier.com/locate/sna

Design and implementation of a sliding-mode controller and a high-gain observer for output tracking of a three-axis pickup

Paul C.-P. Chao [a,*], Chien-Yu Shen [b]

[a] *Department of Electrical and Control Engineering, National Chiao-Tung University, Hsinchu, Taiwan 300, ROC*
[b] *Department of Mechanical Engineering, R&D Center for Membrane Technology, Chung-Yuan Christian University, Chung-Li, Taiwan 32023, ROC*

Received 18 January 2006; received in revised form 19 June 2006; accepted 29 July 2006
Available online 12 September 2006

Abstract

A novel decoupling actuation scheme applied to a new three-axis four-wire optical pickup is synthesized in this study based on theories of sliding-mode control and high-gain observer. The three-axis pickup owns the capability to move the lens holder in three directions of focusing, tracking and tilting. This capability is required particularly for higher data-density optical disks to annihilate the non-zero lens tilting. To achieve control design, Lagrange's equations are first employed to derive equations of motion for the lens holder. A sliding-mode controller is then designed to perform dynamic decoupling and nonlinearity cancellation with the aims of precision tracking, focusing and no tilting. A full-order high-gain observer is next forged to estimate the velocities of the moving lens holder in order to provide low-noised feedback velocity signals for the designed sliding-mode controller. Simulations are carried out to choose appropriate parameter values of the designed controller and observer. Finally, experiments are conducted to validate the effectiveness of the controller for annihilating lens tilting and the capability of the observer for reducing the effects of digital noises on pickup positionings.

Keywords: Three-axis optical pickup; Sliding-mode controller; High-gain observer

1. Introduction

Optical disk drives (ODDs) serve as data-reading platforms for various applications such as CD-ROM, DVD, CDP, LDP, etc. One of key components in optical disk drives is the pickup, which performs data-reading via a well-designed optical system installed inside the pickup. Fig. 1 shows a photo of a three-axis four-wire type pickup actuator, which is designed and manufactured by the Industrial Technology and Research Institute, Taiwan (ITRI). This pickup consists mainly of an objective lens, a lens holder (often called "bobbin"), wire springs, sets of wound coils and permanent magnets. Thanks to flexibility of wire springs, the bobbin could easily be in motion as the forces acting on the bobbin are generated by the electromagnetic interactions between the magnetic fields induced by permanent magnets and the currents conducted in sets of coils. A conventional pickup actuator (not the three-axis one shown in Fig. 1) often owns only two sets of wound coils—the focusing and tracking coils. In this way, two independent actuating forces are generated in the directions of focusing (vertical) and tracking (horizontal to the disk) to perform precision positioning of the lens. This type of actuator is therefore named as "a two-axis actuator".

Large numerical apertures (NA) and/or short wavelength lasers are recently employed for objective lens design in pickups in order to produce a smaller optical detecting spot on an optical disk for better data-reading resolution. This aims at increasing data density of an optical disk via decreasing the circular radius of the aberration region of the optical spot, the main factor limiting resolution of data storage for disks. As the size of the optical spot is decreased, some original electro-mechanical designs of the pickup structure might become obsolete. One of critical challenges arises from the unavoidable tilting of the bobbin during its motion [1]. This tilting is caused by an uneven magnetic field and/or by the fact that the net electromagnetic force in the directions of focusing and tracking do not act through the mass center of the bobbin while the bobbin moves from its static position to

* Corresponding author. Tel.: +886 3 2654310; fax: +886 3 2654358.
E-mail address: pchao@cycu.edu.tw (P.C.-P. Chao).

0924-4247/$ – see front matter © 2006 Elsevier B.V. All rights reserved.
doi:10.1016/j.sna.2006.07.034

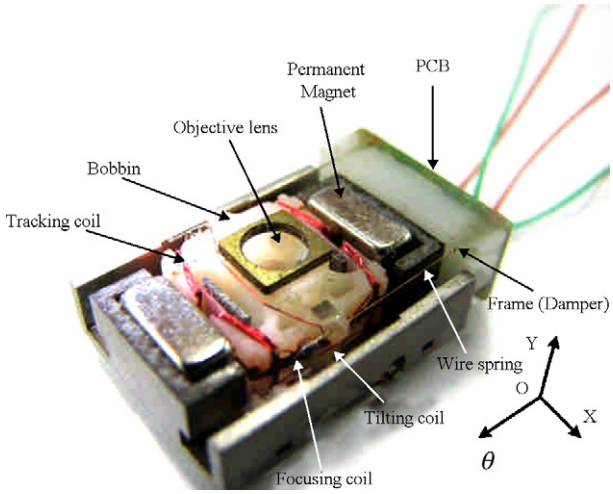

Fig. 1. Structure of the three-axis four-wire type optical pickup by ITRI.

desired vertical and radial positions, resulting in a tilting moment on the bobbin and then a non-zero tilt angle of the bobbin. This non-zero tilting of the bobbin inevitably results in larger levels of distortion on the supposedly circular detecting spot. The spot distortion was originally tolerable for a lower data-resolution design; however, as higher data density of discs is in demand, the level of the spot distortion needs to be restrained for a more accurate, faster data-reading. To this end, the tilting control of the bobbin provides an effective means to minimize the level of the spot distortion. Some three-axis pickups with an additional pair of coils, including the one by ITRI as shown in Fig. 1, were designed recently by researchers to create the servo capability of the bobbin in the tilting direction [2–6]. These actuator structures own the capability of suppressing the unavoidable tiltings of the bobbin in the pickup.

With the hardware of the three-axis pickup well developed, a three degree-of-freedom (DOF) nonlinear controller based on the exact nonlinear dynamic model of the moving bobbin is designed in this study to forge the actuating forces and moment required to perform precision positionings in focusing, tacking and tilting simultaneously. To this end, Lagrange's equations are first applied to system kinetic and potential energies for deriving nonlinear system equations of motion, which is followed by designing a robust sliding-mode control (SMC) [7,8] with considerations of parameter uncertainties and external vibratory disturbances satisfying the input matching condition [8,9]. Note that thanks to the capabilities of first counteracting the known system nonlinearity and then augmenting an artificial tunable switching part in the controller to approach the desired states, the general advantages brought by the SMC over other control designs (such as well-known H^∞ control), are the abilities to directly tackle system nonlinearity, control convergence speed and offer a less complicated design procedure. Along with the SMC is a high-gain observer [10–16] synthesized in this study for the pickup to estimate the feedback moving velocities of the bobbin in the directions of focusing, tracking and tilting. The employment of the high-gain observer is aimed to avoid the high differentiation noises caused by the computer discretizations in practical implementations. Note that most of the high-gain observers were originally designed to estimate the velocities of the robots [12,14–16], since joint velocities are usually measured by noise-contaminated tachometers. With the controller and observer designed theoretically, experiments are conducted to verify the effectiveness of the designed SMC for annihilating bobbin tilting and the capability of the observer for reducing the effects of digital noises on pickup positionings.

This paper is organized as follows. Section 2 presents the mathematical modeling of the three-axis four-wire-type lens actuator. Section 3 presents the design of the sliding-mode controller, while Section 4 does the synthesis of the full-order high-gain observer. The numerical and experimental results are presented in Sections 5 and 6, respectively, to predict and verify the effectiveness of the proposed controller/observer scheme. Finally, conclusions are given in Section 7.

2. Mathematical modeling

A typical three-axis pickup actuator designed ad fabricated by ITRI as shown in Fig. 1 is considered in this study. This pickup mainly consists of a lens holder—bobbin, inner/outer yokes, four wire springs, coils for actuations in directions of tracking/focusing/tilting, four permanent magnets and a PCB holder. To actuate the pickup, three external voltages are applied independently across the respective spring wires to generate the wire-carried currents through the magnetic fields posed by surrounding magnets. This would induce electromagnetic forces and moment on the bobbin for generating necessary motions for precision positioning in the directions of tracking, focusing and tilting. The resulted motion of the objective lens on the bobbin up to expectations makes possible fast, correct data-reading.

2.1. Dynamic modeling of the bobbin

The conventional bobbin, due to its specially designed supporting structure of four parallel wires, exhibits motions mainly in the directions of tracking (*X-axis*) and focusing (*Y-axis*). In addition to the motions in X and Y directions, small tilting often occurs about (θ-*axis*), which is caused by manufacturing tolerance, uneven magnetic fields and/or geometric mis-passes of the electro-magnetic forces acting line on the bobbin mass center. The objective of this study is to design a controller that owns three independent actuating forces and moment in X, Y and θ directions in order to perform precision focusing/tracking and to simultaneously achieve zero tilting to avoid any errors in optical reading signals. The design of such controller starts with an establishment of the system dynamic model. It is first assumed that the pickup assembly can be simply modeled as a lumped mass-spring-damper system due to bobbin's high material rigidity compared to the flexibility of the suspending wires. Fig. 2 shows the schematic bobbin from planar view and accompanying coordinates/notations defined for capturing the bobbin motion from the viewpoint toward the X–Y plane. As seen in this figure are coordinates xyz defined as the body-fixed ones to the moving bobbin, while coordinates XYZ are global, ground coordinates. X also serves as a dynamic variable, capturing the horizontal, tracking motion; Y does the vertical, focusing

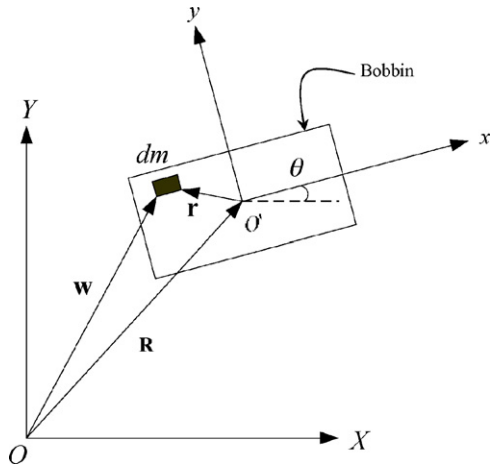

Fig. 2. Planar dynamic model of the bobbin.

motion; θ does the rotating angle of the bobbin about Z, i.e. the tilting angle. The displacement vector $\mathbf{w}$ for a given point of the bobbin can be captured by

$$\mathbf{w} = \mathbf{R} + \mathbf{T}\mathbf{r} \tag{1}$$

where $\mathbf{R} = [\,X \quad Y \quad \theta\,]^{\mathrm{T}}$ is the position vector of bobbin centroid, O', measured from the origin of the ground coordinates XYZ, O. Also,

$$\mathbf{T} = \begin{bmatrix} \cos\theta & -\sin\theta & 0 \\ \sin\theta & \cos\theta & 0 \\ 0 & 0 & 1 \end{bmatrix}$$

is the transformation matrix due to θ, and $\mathbf{r_o} = [\,x \quad y \quad \theta]$ is the position vector of the centroid o. Differentiating Eq. (1) with respect to time and put into kinetic energy, the kinetic energy of the bobbin can be obtained as

$$\begin{aligned} L_{\mathrm{T}} &= \frac{1}{2}\int_m \dot{\mathbf{w}}^{\mathrm{T}}\dot{\mathbf{w}}\,\mathrm{d}m \\ &= \frac{1}{2}m(\dot{X}^2 + \dot{Y}^2) + \frac{1}{2}I_{O\theta}\dot{\theta}^2 - \dot{X}\dot{\theta}(I_x\sin\theta + I_y\cos\theta) \\ &\quad + \dot{Y}\dot{\theta}(I_x\cos\theta - I_y\sin\theta), \end{aligned} \tag{2}$$

where $I_{O\theta}$ is the mass moment of inertia of the bobbin about its centroid along z axis, while $I_x = \int_m x\,\mathrm{d}m$ and $I_y = \int_m y\,\mathrm{d}m$ are first mass moments of inertia with respect to x and y axes, respectively. The potential energy of the pickup is next expressed as

$$V = \frac{1}{2}(k_x X^2 + k_y Y^2 + k_\theta\theta^2) + mgY, \tag{3}$$

where k_x, k_y and k_θ are the equivalent spring stiffnesses to the bobbin in tracking, focusing and tilting directions; m the mass of bobbin; g is the gravitation. Finally, the non-conservative virtual work can be derived as

$$\begin{aligned} \delta W &= \int_A (\mathbf{T}\cdot\mathbf{F})^{\mathrm{T}}\delta\mathbf{w}\,\mathrm{d}A = (F_x\cos\theta - F_y\sin\theta)\delta X \\ &\quad + (F_x\sin\theta + F_y\cos\theta)\delta Y + F_\theta\delta\theta, \end{aligned} \tag{4}$$

where δW denotes virtual work while F_x and F_y represent the actuation forces acting on the centroid, respectively, in the tracking and focusing directions. F_θ denotes the torsional moment about θ. Substituting Eqs. (2)–(4) into Lagrange's equation [17], the equations of motion can be readily obtained as

$$\mathbf{M}\ddot{\mathbf{q}} + \mathbf{K}_0\mathbf{q} + \mathbf{N} + \mathbf{G} = \mathbf{T}\mathbf{F}, \tag{5}$$

where $\mathbf{q} = [\,X \quad Y \quad \theta\,]^{\mathrm{T}}$ contains the generalized coordinates for describing the motion of the bobbin. $\mathbf{M}$ and $\mathbf{K}_0$ are overall mass and stiffness matrices. $\mathbf{N}$ contains the centrifugal and Coriolis force terms. $\mathbf{G}$ captures the gravitational effect. $\mathbf{F}$ captures the actuator forces. Their expressions are given in the followings:

$$\mathbf{M} = \begin{bmatrix} m & 0 & -(I_x\sin\theta + I_y\cos\theta) \\ 0 & m & (I_x\cos\theta - I_y\sin\theta) \\ -(I_x\sin\theta + I_y\cos\theta) & (I_x\cos\theta - I_y\sin\theta) & I_{0\theta} \end{bmatrix},$$

$$\mathbf{K}_0 = \mathbf{diag}[\,k_x \quad k_y \quad k_\theta\,], \quad \mathbf{F} = [\,F_x \quad F_y \quad F_\theta\,]^{\mathrm{T}}$$

$$\mathbf{G} = [\,0 \quad mg \quad 0\,]^{\mathrm{T}},$$

$$\mathbf{N} = \begin{bmatrix} -\dot{\theta}^2(I_x\cos\theta - I_y\sin\theta) \\ -\dot{\theta}^2(I_x\sin\theta + I_y\cos\theta) \\ \dot{X}\dot{\theta}(I_x\cos\theta - I_y\sin\theta) + \dot{Y}\dot{\theta}(I_x\sin\theta + I_y\cos\theta) \end{bmatrix}.$$

The stiffness coefficients in the above $\mathbf{K}_0$, (k_x, k_y) comply with

$$k_x = k_y = 4\cdot\frac{12EI_{\mathrm{w}}}{L^3}, \tag{6}$$

where E is the elastic modulus, I_{w} the area moment of inertia about x or y axis for the wire and L is the length of each wire. The expression of k_θ is next due to be derived. To this end, Fig. 3 are first depicted to illustrate how to derive the moment M responsible for the tilting of the bobbin. In Fig. 3, F represents the combined electro-magnetic force in focusing and tracking directions, which is generated by the current carried by a wire at some instant. ϕ is the angle between F and x axis. Assuming an even magnetic field, the electro-magnetic forces induced by other three wires are identical and can also then be denoted by F. Then the net moment acting on the bobbin is

$$M = 4FD,$$

where D, as shown in Fig. 3(b), is the distance between the bobbin center and the wire. The angular deflection θ is next derived for calculating the equivalent rotational (tilting) stiffness k_θ, which is started with expressing the translational deflections in x and y directions due to the total electro-magnetic force F as

$$\delta_x = \frac{4F\cos\phi}{k_x} = \frac{F\cos\phi L^3}{12EI_{\mathrm{w}}} \quad \text{and}$$

$$\delta_y = \frac{4F\sin\phi}{k_y} = \frac{F\sin\phi L^3}{12EI_{\mathrm{w}}}. \tag{7}$$

The net deflection along F is

$$\delta = \sqrt{\delta_x^2 + \delta_y^2}. \tag{8}$$

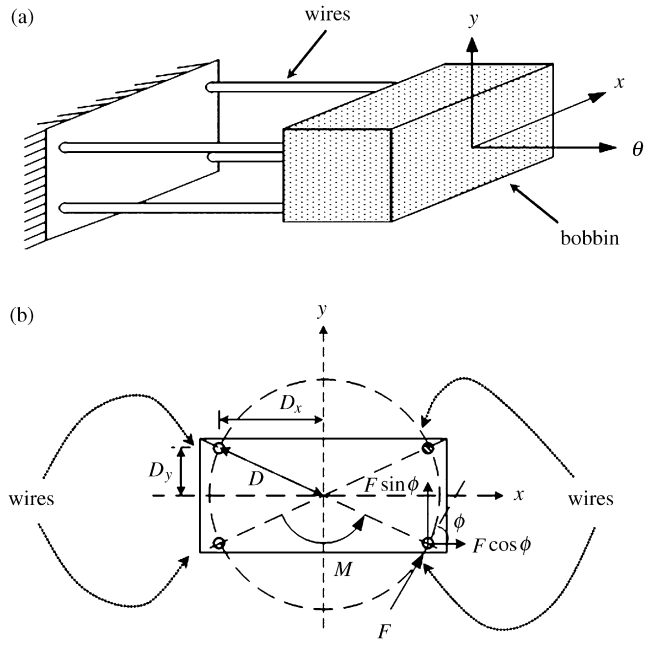

Fig. 3. Moment generation of the four-wire-type optical pickup. (a) 3D view and (b) side view of the bobbin from positive θ direction.

Assuming small motions of the bobbin, thus, $\delta = D\theta$. Henceforth,

$$k_\theta = \frac{M}{\theta} = \frac{4FD}{\delta/D} = \frac{48EI_w(D_x^2 + D_y^2)}{L^3\sqrt{(D_x/D)^2 + (D_x/D)^2}}, \tag{9}$$

where D_x and D_y are, respectively as shown in Fig. 3(b), the distances in x and y directions between the bobbin center and each wire.

2.2. Modeling of voice coil motors

The electro-magnetic forces acting on the bobbin in the directions of focusing, tracking and tilting are parameterized in this section. The actuators composed of sets of coils in the pickup are namely voice coil motors (VCMs), the electromagnetic dynamic balances of which in pickup operation, as equivalently shown in Fig. 4, can be derived based on the Kirchhoff's law, yielding

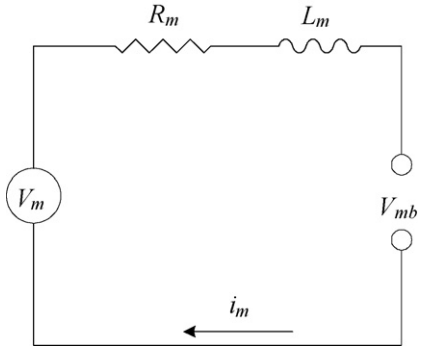

Fig. 4. Circuit model of the voice coil motor.

$$\begin{aligned} V_{m(x,y,\theta)} &= R_m \cdot i_m + L_m \frac{\mathrm{d}i_m}{\mathrm{dt}} + V_{mb} \\ &= R_m \cdot i_m + L_m \frac{\mathrm{d}i_m}{\mathrm{dt}} K_{mvs} \cdot \dot{q}_{(x,y,\theta)}, \end{aligned} \tag{10}$$

where $V_{m(x,y,\theta)}$ are the independent VCM input voltages in three directions, V_{mb} is the back electromotive force (EMF) and $\{R_m, i_m, L_m$ and $K_{mvs}\}$ represent the resistance, current, inductance and back EMF constant of the VCMs, respectively. With the electrical dynamics in Eq. (10) derived, the Fleming's left hand rule [18] is then employed to derive the electro-magnetic forces for actuation, which is

$$\begin{aligned} F_{(x,y,\theta)} &= n_m \cdot B_m \cdot l_m \cdot i_m, = \left(\frac{n_m \cdot B_m \cdot l_m}{R_m}\right) \\ &\times \left(V_{m(x,y,\theta)} - L_m \frac{\mathrm{d}i_m}{\mathrm{d}t} - K_{mvs} \cdot \dot{q}_{(x,y,\theta)}\right), \end{aligned} \tag{11}$$

where n_m is the number of coil loops, B_m is the magnetic flux density within the air gap between the bobbin and magnets, and l_m is the total effective coil length for a single coil loop. Based on the fact that the electrical dynamics of the conducted current is much faster than those mechanical ones in the directions of focusing, tracking and tilting, the term $L_m(\mathrm{d}i_m/\mathrm{d}t)$ in Eq. (11) can be neglected. Incorporating further the simplified $F_{(x,y,\theta)}$ in Eq. (11) into the system model in Eq. (5) arrives at a net system model with additional consideration of wire damping as

$$\mathbf{M}\ddot{\mathbf{q}} + \mathbf{C}_0\dot{\mathbf{q}} + \mathbf{K}_0\mathbf{q} + \mathbf{N} + \mathbf{G} = \overline{\mathbf{T}}_0\mathbf{V}, \tag{12}$$

where $\mathbf{V}$ is of the form $\mathbf{V} = [\,V_x \quad V_y \quad V_\theta\,]^{\mathrm{T}}$ which contains the input voltages into the VCMs in three DOFs of tracking, focusing and tilting, respectively. The remaining two expressions in Eq. (12), $\mathbf{C}_0$ and $\overline{\mathbf{T}}_0$, are given as follows:

$$\mathbf{C}_0 = \begin{bmatrix} C_x + \left(\dfrac{n_x B_x l_x}{R_x}\right) K_{mvs,x} & 0 & 0 \\ 0 & C_y + \left(\dfrac{n_y B_y l_y}{R_y}\right) K_{mvs,y} & 0 \\ 0 & 0 & C_\theta + \left(\dfrac{n_\theta B_\theta l_\theta}{R_\theta}\right) K_{mvs,\theta} \end{bmatrix}, \tag{13a}$$

$$\overline{\mathbf{T}}_0 = \begin{bmatrix} \cos\theta \cdot \dfrac{n_x B_x l_x}{R_x} & -\sin\theta \cdot \dfrac{n_y B_y l_y}{R_y} & 0 \\ \sin\theta \cdot \dfrac{n_x B_x l_x}{R_x} & \cos\theta \cdot \dfrac{n_y B_y l_y}{R_y} & 0 \\ 0 & 0 & \dfrac{n_\theta,\, B_\theta,\, l_\theta}{R_\theta} \end{bmatrix}. \tag{13b}$$

2.3. Modeling of uncertainties and disturbance

There often exist an uneven magnetic filed generated by magnets and manufacturing tolerances with respects to various crucial dimensions of the pickup structure, which are the factors, other than the movement of the bobbin, causing the mis-passes of the electro-magnetic forces on the mass center of the bobbin; as results, it leads to a non-zero tilting. For later control design, the uncertainties due to the uneven magnetic field and manufacturing tolerance are formulated into the mathematical model in Eq. (12) as structured, parametric uncertainties [19]. The formulation is started with re-expressing the system equation in Eq. (12) as

$$\mathbf{M}\ddot{\mathbf{q}} + \mathbf{C}\dot{\mathbf{q}} + \mathbf{K}\mathbf{q} + \mathbf{N} + \mathbf{G} = \overline{\mathbf{T}}\mathbf{V}, \tag{14}$$

where

$$\mathbf{M} = \mathbf{M}_0, \qquad \mathbf{N} = \mathbf{N}_0, \qquad \mathbf{G} = \mathbf{G}_0, \tag{15}$$

$$\mathbf{C} = \mathbf{C}_0 + \mathbf{C}_\Delta, \qquad \mathbf{K} = \mathbf{K}_0 + \mathbf{K}_\Delta, \qquad \overline{\mathbf{T}} = \overline{\mathbf{T}}_0 + \overline{\mathbf{T}}_\Delta, \tag{16}$$

where subscripts of "0" denotes the nominals while "Δ" denotes the corresponding parametric variations due to the uneven magnetic field and manufacturing tolerance. Note that no variation components are associated with $\mathbf{M}$, $\mathbf{N}$, $\mathbf{G}$, since they can be measured or derived with relative precision. On the other hand, based on the geometry of the bobbin, the variations $\mathbf{C}_\Delta$, $\mathbf{K}_\Delta$ and $\overline{\mathbf{T}}_\Delta$ can be modeled by

$$\mathbf{C}_\Delta = \begin{bmatrix} 0 & 0 & 0 \\ 0 & 0 & 0 \\ \left(\dfrac{n_x B_x l_x}{R_x}\right) K_{mvs,x} \cdot \Gamma_y & \left(\dfrac{n_y B_y l_y}{R_x}\right) K_{mvs,y} \cdot \Gamma_x & 0 \end{bmatrix}, \tag{17a}$$

$$\mathbf{K}_\Delta = \begin{bmatrix} 0 & 0 & k_x a_y \\ 0 & 0 & k_y a_x \\ k_x a_y & k_y a_x & k_x a_y^2 + k_y a_x^2 \end{bmatrix}, \tag{17b}$$

$$\overline{\mathbf{T}}_\Delta = \begin{bmatrix} 0 & 0 & 0 \\ 0 & 0 & 0 \\ \dfrac{n_x B_x l_x}{R_x} \cdot \Gamma_y & \dfrac{n_y B_y l_y}{R_y} \cdot \Gamma_x & 0 \end{bmatrix}, \tag{17c}$$

where a_x and a_y are the equivalent asymmetric offsets of the restoring forces induced by the supporting stiffnesses k_x and k_y, respectively. These non-zero a_x and a_y are caused by relative misalignments and/or manufacturing tolerances of pickup components. On the other hand, Γ_x and Γ_y are the offsets of the electromagnetic force acting lines from the mass center of the bobbin due to an uneven magnetic field and/or misalignments of magnetic components in x and y directions, respectively. In this study, parametric uncertainties of $\{a_x, a_y, \Gamma_x, \Gamma_y\}$ are assumed approximately up to 5% of the respective sizes of the bobbin.

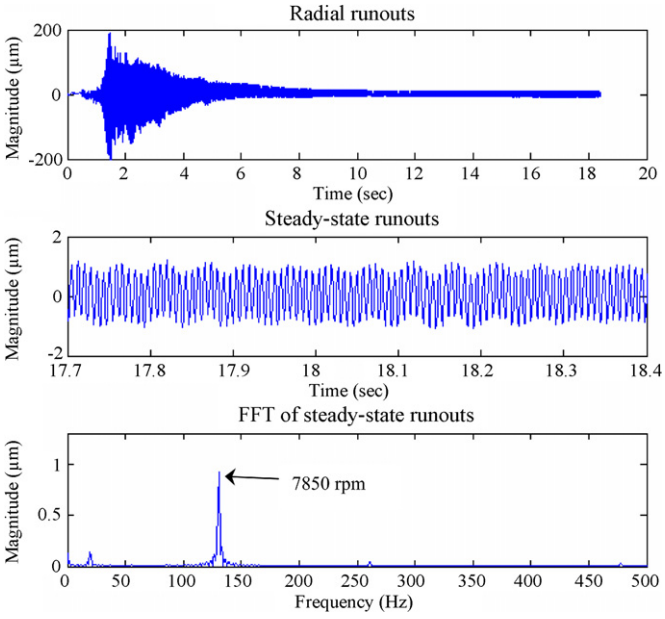

Fig. 5. Time trace and FFT of measured runouts.

The external disturbances are next modeled based on realistic radial vibrations (runouts) for later control design. To this end, a simple experiment system is built with mainly a commercial optical disc drive in the laboratory to mimic the aforementioned CD-ROM system, and two laser sensors to measure the radial vibrations. The measured radial vibrations are shown in time and frequency domains in Fig. 5, where it is seen that the practical radial vibratory disturbance consists of a primary harmonic of 1 μm at 7850 rpm, which is exactly the disk rotational frequency. These measured radial vibrations would serve as output disturbances in later control design and experimental validation. Incorporating the measured disturbance into system Eq. (14) arrives at the modified system equations as

$$\mathbf{M}\ddot{\mathbf{q}} + \mathbf{C}\dot{\mathbf{q}} + \mathbf{K}\mathbf{q} + \mathbf{N} + \mathbf{G} + \tilde{\mathbf{D}} = \overline{\mathbf{T}}\mathbf{V}, \tag{18}$$

where $\tilde{\mathbf{D}} = [\, v_{d,x} \quad v_{d,y} \quad 0\,]^{\mathrm{T}} \cdot v_{d,x}$ and $v_{d,y}$ are assumed as the aforementioned measured radial vibrations in x and y directions, respectively.

3. Controller design

A sliding-mode controller (SMC) is synthesized in this section for precision positioning of the pickup actuator in 3 DOFs. A well-designed SMC is expected to accept the estimated states of $\mathbf{q}$ and $\dot{\mathbf{q}}$ from the high-gain observer designed in the next section, and then to calculate required control efforts $\mathbf{V}$ to be fed to the optical pickup. Fig. 6 shows a block diagram that well illustrates the structure of the SMC and the accompanied high-gain observer. To complete SMC design, it is first understood that the systems controlled by a SMC are a class of controlled nonlinear systems actuated by discontinuous control efforts, which change the system structure to have the controlled states reaching and leaving the switching surface (or sliding surface). The structure of the switching surface is specified at the zeros of a so-called

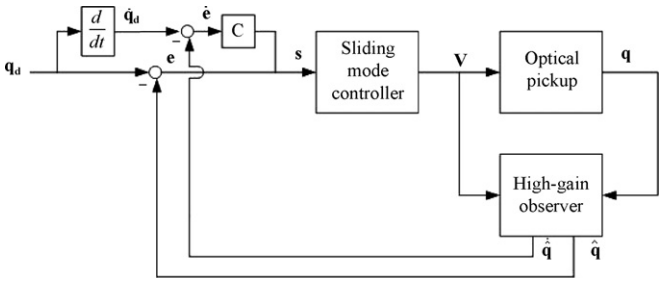

Fig. 6. Block diagram of the controlled system with the observer.

"switching function," which is a pre-defined vector-valued function, often denoted by $\mathbf{S}(\mathbf{e})$. The sign of the switching function indicates which side of the switching surface the states are, and offers the direction for the control action to be designed. In this section, the objective is to design the switching surface reaching law for the SMC design. This is accomplished by determining the reaching mode and the overall control law, which is aimed at the convergence of the system dynamic to the switching surface and ultimately the desired states. To this goal, three independent control inputs to the three-axis four-wire type optical pickup are synthesized to accomplish precision positioning in tracking/focusing and annihilating tilting. This starts with re-writing Eq. (18) as

$$\ddot{\mathbf{q}} = -\mathbf{M}^{-1}\mathbf{C}\dot{\mathbf{q}} - \mathbf{M}^{-1}\mathbf{K}\mathbf{q} - \mathbf{M}^{-1}\mathbf{D} + \mathbf{M}^{-1}\bar{\mathbf{T}}\mathbf{V}, \tag{19}$$

where $\mathbf{D} = (\mathbf{N} + \mathbf{G} + \tilde{\mathbf{D}})$. The error vector of the system is defined as

$$\mathbf{e} = \mathbf{q} - \mathbf{q_d} = \begin{bmatrix} X - X_d \\ Y - Y_d \\ \theta - \theta_d \end{bmatrix}, \tag{20}$$

where $\mathbf{q_d} = [\, X_d \quad Y_d \quad \theta_d \,]^{\mathrm{T}}$ are targeted focusing, tracking and tilting positions. Note that to eliminate non-zero tilting, θ_d is set as zero. A switching vector function $\mathbf{S}(\mathbf{e})$ containing the integrals of the positioning errors is next defined as

$$\mathbf{S}(\mathbf{e}) = \left(\frac{\mathrm{d}}{\mathrm{d}t} + \mathbf{C}_1\right)^2 \left(\int_0^t \mathbf{e}\,\mathrm{d}t\right) = \dot{\mathbf{e}} + 2\mathbf{C}_1\mathbf{e} + \mathbf{C}_1^{\mathrm{T}}\mathbf{C}_1 \int_0^t \mathbf{e}\,\mathrm{d}t, \tag{21}$$

where $\mathbf{C}_1 = \mathbf{diag}[\, C_{1,x} \quad C_{1,y} \quad C_{1,\theta} \,]$. Note that $\mathbf{C_1}$ is a matrix with positive diagonal elements to be determined. The determination of the elements in $\mathbf{C_1}$ decides relative convergence speeds among 3 DOFs. Taking time derivative of $\mathbf{S}(\mathbf{e})$ in Eq. (21) and also incorporating Eqs. (19) and (20) leads to

$$\dot{\mathbf{S}} = (-\mathbf{M}^{-1}\mathbf{C}\dot{\mathbf{q}} - \mathbf{M}^{-1}\mathbf{K}\mathbf{q} - \mathbf{M}^{-1}\mathbf{D} + \mathbf{M}^{-1}\bar{\mathbf{T}}\mathbf{V}) - \ddot{\mathbf{q}}_\mathbf{d} + 2\mathbf{C}_1(\dot{\mathbf{q}} - \dot{\mathbf{q}}_\mathbf{d}) + \mathbf{C}_1^2(\mathbf{q} - \mathbf{q}_\mathbf{d}). \tag{22}$$

To find an appropriate control law, the reaching law of the states with proportional plus constant power rates in the form of

$$\dot{\mathbf{S}} = -P\mathbf{S} - \mathbf{Q}\mathrm{sgn}(\mathbf{S}), \tag{23}$$

is first set to be achieved. Note that $\mathbf{Q} = W \cdot [\, |S_x|^\alpha \quad |S_y|^\alpha \quad |S_\theta|^\alpha \,]^{\mathrm{T}}$ with S_x, S_y, S_θ being the components of given sliding-mode matrix $\mathbf{S}$. Furthermore, P and W are positive weighting coefficients to be designed, while the choice of α also allows one to adjust the convergence speeds. By selecting appropriate values of P, W and α in Eq. (23), the convergence of state trajectories to the switching surface can be guaranteed since the reaching law (23) directly leads to

$$\mathbf{S} \cdot \dot{\mathbf{S}} < 0. \tag{24}$$

To make possible the reaching law (23), the control efforts $\mathbf{V}$ in Eq. (22) can be designed as follows, based on theory of sliding-mode control,

$$\mathbf{V} = \begin{bmatrix} V_x & V_y & V_\theta \end{bmatrix} = (\mathbf{M}^{-1}\bar{\mathbf{T}}_0)^{-1} \left(\mathbf{M}^{-1}\mathbf{C}_0\dot{\mathbf{q}} + \mathbf{M}^{-1}\mathbf{K}_0\mathbf{q} + \ddot{\mathbf{q}}_\mathbf{d} - \mathbf{C}_1\dot{\mathbf{q}} + \mathbf{C}_1\dot{\mathbf{q}}_\mathbf{d} - P\mathbf{S} - \mathbf{Q}\mathrm{sgn}(\mathbf{S}) + \mathbf{C}_1^{\mathrm{T}}\mathbf{C}_1 \int_0^t (\mathbf{q} - \mathbf{q}_\mathbf{d})\mathrm{d}t \right). \tag{25}$$

Note herein that by selecting large values of P and W for the control effort $\mathbf{V}$ in Eq. (25), one is able to not only reach the convergence in Eq. (24) but also retain the robustness against the uncertainties of $\boldsymbol{C}_\Delta$, $\boldsymbol{K}_\Delta$ and $\boldsymbol{T}_\Delta$ as prescribed in Eq. (17) and the disturbance $\mathbf{D}$ specified in Eq. (18). Note that the necessary condition for reaching the robustness against the uncertainties and disturbance by the voltage input $\mathbf{V}$ in Eq. (25) is the satisfaction of the input matching condition [8,9]. Appendix A details the proof on the satisfaction. Finally, in order to reduce the known chattering phenomenon near the switching surface, the function sgn(s) pre-proposed in Eq. (25) is replaced by a saturation function inside the pre-designated boundary layer [7]. The saturation function is of the form

$$\mathrm{sat}(\mathbf{S}) = \begin{Bmatrix} \mathrm{sgn}(\mathbf{S}), & \text{if } |\mathbf{S}| > \phi_\mathrm{s} \\ \dfrac{\mathbf{S}}{\phi_\mathrm{s}}, & \text{if } |\mathbf{S}| \le \phi_\mathrm{s} \end{Bmatrix}, \tag{26}$$

where ϕ_s is the boundary layer width of the switching surface.

4. Observer design

With the sliding-mode controller designed, a high-gain observer is synthesized and augmented into the controlled system in this section with the aim to estimate the moving velocities of the bobbin in the directions of tracking, focusing and tilting. The estimated velocities would be provided to the controller as the feedback signals in places of those digitally computed time derivatives from the measured displacements of the moving lens/bobbin. The replacements are motivated by the fact that the computed derivatives are often contaminated by the noises caused by sensor limitation and magnified by consequent digital discretization.

The design process of the high-gain observer follows the procedure similar to that in [10], which starts with defining new state and output variables of the system as $\mathbf{q}_1 = \mathbf{q}$, $\mathbf{q}_2 = \dot{\mathbf{q}}$ and $\mathbf{y} = \mathbf{q}$. With these new definitions, the system equations augmented with the designed sliding-mode controller in Eq. (19) can be

re-expressed as

$$\dot{\mathbf{q}}_1 = \mathbf{q}_2, \qquad \dot{\mathbf{q}}_2 = f(\mathbf{q}_1, \mathbf{q}_2) + g(\mathbf{q}_1)\mathbf{V}, \qquad \mathbf{y} = \mathbf{q}_1, \tag{27}$$

where $f(\mathbf{q}_1, \mathbf{q}_2) = -\mathbf{M}^{-1}\mathbf{C}_0\mathbf{q}_2 - \mathbf{M}^{-1}\mathbf{K}_0\mathbf{q}_1 - \mathbf{M}^{-1}\mathbf{D}$, $g(\mathbf{q}_1) = \mathbf{M}^{-1}\overline{\mathbf{T}}_0$, and $\mathbf{y} = \mathbf{q}_1 = [X \quad Y \quad \theta]$. Note that $\mathbf{y} = [X \quad Y \quad \theta]$ is the output vector containing the measured displacements of the moving bobbin in three DOFs of focusing, tacking and tilting. With the sliding-mode control effort designed previously by Eq. (25), the term $\mathbf{V}$ in Eq. (27) can be seen as a function of state estimations offered by the observer and time, i.e. $\mathbf{V} = \eta(\hat{\mathbf{q}}_1, \hat{\mathbf{q}}_2, \mathbf{t})$ where $\hat{\mathbf{q}}_1$ and $\hat{\mathbf{q}}_2$ denote, respectively, the estimates of the actual displacements and velocities of the bobbin/lens, $\mathbf{q}_1$ and $\mathbf{q}_2$, respectively. Thus the system Eq. (27) can be further simplified as

$$\dot{\mathbf{q}}_1 = \mathbf{q}_2, \qquad \dot{\mathbf{q}}_2 = \phi(\mathbf{q}_1, \mathbf{q}_2, \hat{\mathbf{q}}_1, \hat{\mathbf{q}}_2, \mathbf{t}), \qquad \mathbf{y} = \mathbf{q}_1, \tag{28}$$

where $\phi(\mathbf{q}_1, \mathbf{q}_2, \hat{\mathbf{q}}_1, \hat{\mathbf{q}}_2, \mathbf{t}) = f(\mathbf{q}_1, \mathbf{q}_2) + g(\mathbf{q}_1)\eta(\hat{\mathbf{q}}_1, \hat{\mathbf{q}}_2, \mathbf{t})$. Consider the high-gain observer in the form of

$$\dot{\hat{\mathbf{q}}}_1 = \hat{\mathbf{q}}_2 + \frac{1}{\varepsilon}\mathbf{H}_\mathrm{p}(\mathbf{y} - \hat{\mathbf{q}}_1), \qquad \dot{\hat{\mathbf{q}}}_2 = \frac{1}{\varepsilon^2}\mathbf{H}_\mathrm{v}(\mathbf{y} - \hat{\mathbf{q}}_1), \tag{29}$$

On the other hand, $\mathbf{H}_\mathrm{p}$ and $\mathbf{H}_\mathrm{y}$ are designated as the diagonal matrices with constant elements, i.e. $\mathbf{H}_\mathrm{p} = \mathbf{diag}(h_{p,i})$ and $\mathbf{H}_\mathrm{v} = \mathbf{diag}(h_{v,i})$, with the aim to achieve an estimation convergence for $\hat{\mathbf{q}}_1$ and $\hat{\mathbf{q}}_2$. Convergence of the estimation can be guaranteed, even against the uncertainties of $\mathbf{C}_\Delta$, $\mathbf{K}_\Delta$ and $\mathbf{T}_\Delta$, by choosing the values of $h_{p,i}$'s and $h_{v,i}$'s such that the spectra (roots) of the characteristic polynomials

$$p_i(\lambda) = \lambda^2 + h_{p,i}\lambda + h_{v,i}, \quad i = 1, \ldots, N \tag{30}$$

are all in the left half plane. Finally, the value of ε in the observer in Eq. (29) is chosen as a small positive parameter, serving as a detuning parameter to adjust the convergence speed of the designed observer. ε is usually detuned small enough such that the convergence speed of the observer is much faster than the targeted convergence speeds of states of the controlled system, resulting in assurance of the expected control performance by the SMC designed in Section 3, where no observer is assumed. On the other hand, note that the smallness of ε in fact leads to large values of $1/\varepsilon$ and $1/\varepsilon^2$ in Eq. (29), explaining why the observer is named the high-gain observer. It is important to note herein as well that the estimated $\hat{\mathbf{q}}_1$ and $\hat{\mathbf{q}}_2$ by the high-gain observer are computed through the time integrations on the right hand sides of Eq. (29), rendering the estimated values of $\hat{\mathbf{q}}_1$ and $\hat{\mathbf{q}}_2$ in lower noises than those embedded in directly computed time-derivatives from measured displacements. With values of $h_{p,i}$'s, $h_{v,i}$'s and ε determined following the aforementioned directives, the convergence of the estimation by the high-gain observer can be guaranteed. The proof to ensure the convergence is provided in Appendix B.

5. Numerical simulations

With the sliding-mode controller and the high-gain observer synthesized, numerical simulations are conducted in this section to find suitable controller parameters and observer gains.

Table 1
Geometric and magnetic parameter values of the VCM actuator

Description	Symbol	Value	Unit
Max voltage	$V_{m(\max)}$	5	Volt
Max current	$i_{m(\max)}$	0.67	A
Resistance	R_x	7.5	Ω
Resistance	R_y	7.5	Ω
Resistance	R_θ	6.4	Ω
Back EMF constant	$K_{mvs,x}$	0.0416	Volt/(m/s)
Back EMF constant	$K_{mvs,y}$	0.0416	Volt/(m/s)
Back EMF constant	$K_{mvs,\theta}$	0.0357	Volt/(m/s)
Magnetic flux density	B_x	0.454	Wb/m^2
Magnetic flux density	B_y	0.454	Wb/m^2
Magnetic flux density	B_θ	0.454	Wb/m^2
Effective length*	l_x	0.37	m
Effective length*	l_y	0.35	m
Effective length*	l_θ	0.1	m
No. of coil loops	n_x	32	Loop
No. of coil loops	n_y	25	Loop
No. of coil loops	n_θ	40	Loop

* The effective lengths of the wires for focusing/tracking/tilting are total lengths of coil loops, not the size of the coils in appearance.

The practical three-axis pickup by ITRI, as shown in Fig. 1, is considered for the ensuing numerical simulations and experimental validation. All parameters of the considered three-axis four-wire type optical pickup actuator are calibrated or obtained from documented properties. They are

$$\begin{aligned} &m = 2.87 \times 10^{-4}\,\mathrm{kg}, \quad L = 12.5 \times 10^{-3}\,\mathrm{m}, \\ &I_w = 1.01 \times 10^{-17}\,\mathrm{m}^4, \quad E = 1.1 \times 10^{11}\,\mathrm{Pa}, r = 4 \times 10^{-5}\,\mathrm{m}, \\ &D_y = 1.225 \times 10^{-3}\,\mathrm{m}, \\ &\Delta t = 5 \times 10^{-4}\,\mathrm{s}, I_{0\theta} = 1.97 \times 10^{-9}\,\mathrm{kg\,m^2}, \\ &I_x = 1.97 \times 10^{-9}\,\mathrm{kg\,m}, \quad I_y = 3.47 \times 10^{-9}\,\mathrm{kg\,m}, \end{aligned} \tag{31}$$

while the parameter values of the voice coil motors (VCMs) are given in Table 1.

5.1. Choosing control parameters

Numerical simulations are carried out in this subsection with the aim to choose appropriate parameter values for the sliding-mode controller designed in Section 3. The appropriateness can be ensured if the error convergence in Eq. (24) is reached with the presences of the disturbances due to radial runouts, as specified by $\mathbf{D}$ in Eq. (18), and the parametric uncertainties $\{a_x, a_y, \Gamma_x, \Gamma_y\}$ in Eq. (17) that are prescribed as 5% of respective dimensions of the pickup bobbin. It can be obtained from the SMC design process proposed in Section 3 that the main control parameters affecting the controller performance are P, W, α and $\mathbf{C_1}$. Among these parameters, one can only consider P and W as the main parameters to be tuned for convergence and robustness, since the effects of α are only on the convergence that can also be tuned by P and W. On the other hand, $\mathbf{C_1}$ determines only the relative convergence speeds among the states. Therefore, in the following process of controller tuning,

α is set to be unity to leave the job of convergence tuning to P and W, while $\mathbf{C_1}$ is designated as $\mathbf{C}_1 = \text{diag}[\,300 \quad 300 \quad 900\,]$ for reflecting desired relative convergence speeds among the states.

Four cases of varied P and W as listed in Table 2 are considered herein for simulations to obtain satisfactory controller performance. The first, second and third cases are integrally set to consider relative large, medium and small levels of P and a fixed W, with the aim to find the most suitable value of P for better control convergence and robustness. With the desired trajectories in x and y directions set to be step functions of 10 μm and the desired tilting in θ direction to be zero, simulations are conducted and then the related results are shown in Figs. 7–9, respectively, corresponding to Cases 1–3 in Table 2. It can be seen from these figures that the case with the pre-chosen medium value of $P = 5 \times 10^4$, as shown in Fig. 8, renders the smallest root

Table 2
Cases for choosing weightings P and W

Case no.	P	W
1	5×10^3	10
2 (also for experiment)	5×10^4	10
3	5×10^5	10
4	5×10^4	10^3

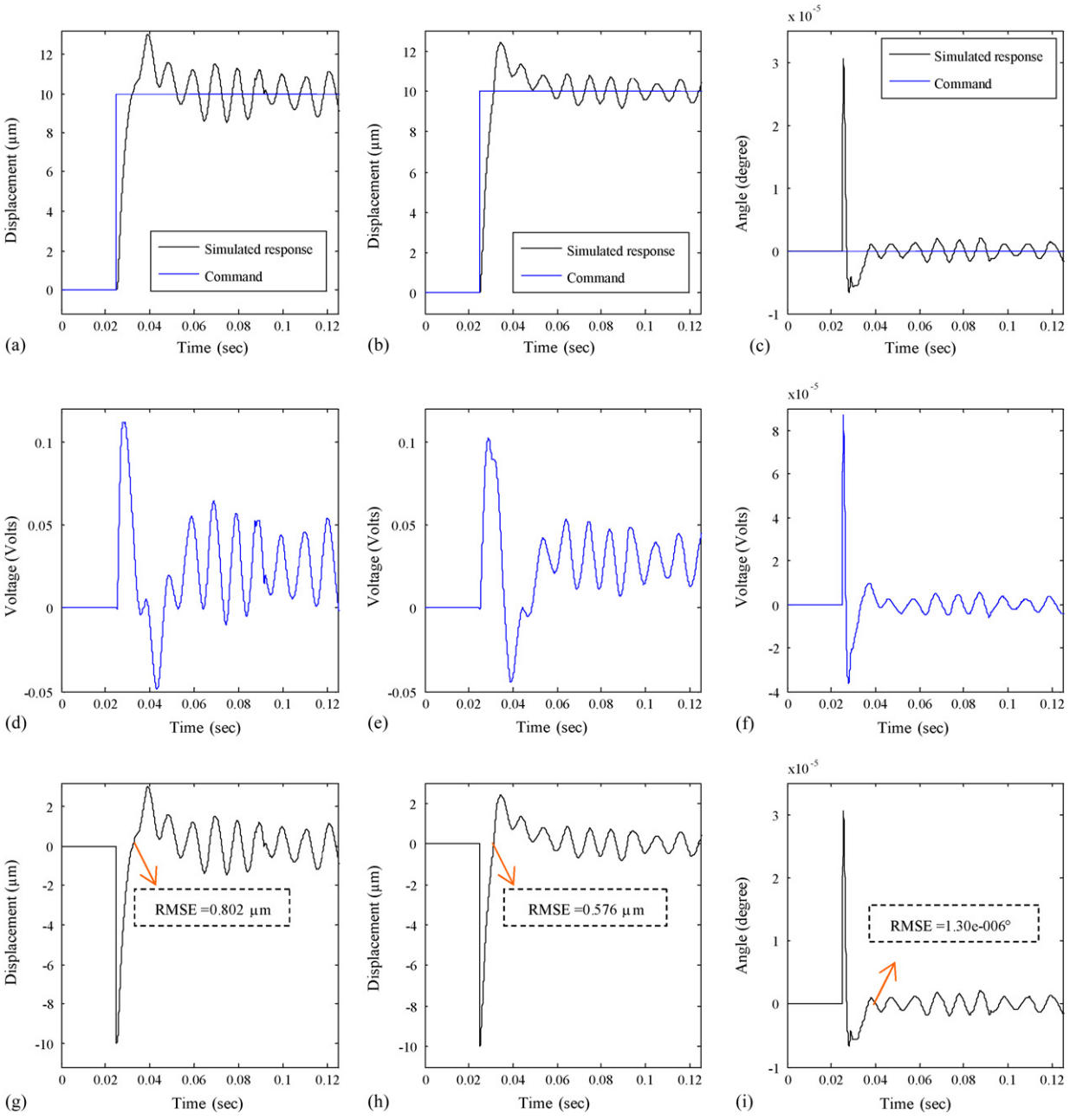

Fig. 7. Simulated step responses, control efforts and errors of the pickup system controlled by the designed SMC in three directions with control parameters of Case 1 given in Table 2. (a) Tracking, (b) focusing, (c) tilting, (d) tracking control effort, (e) focusing control effort, (f) tilting control effort, (g) tracking error, (h) focusing error and (i) tilting error.

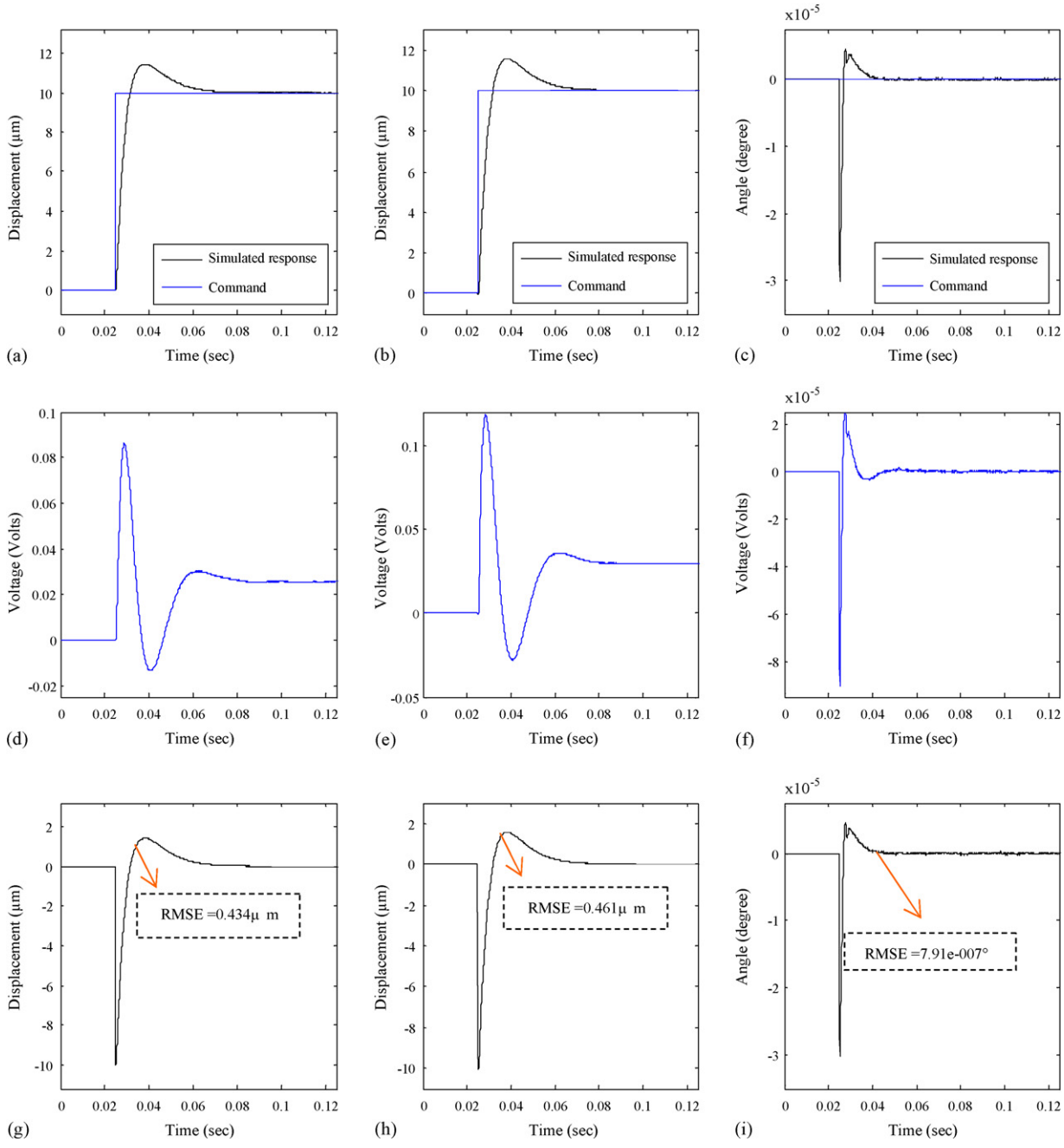

Fig. 8. Simulated step responses, control efforts and errors of the pickup system controlled by the designed SMC in three directions with control parameters of Case 2 given in Table 2. (a) Tracking, (b) focusing, (c) tilting, (d) tracking control effort, (e) focusing control effort, (f) tilting control effort, (g) tracking error, (h) focusing error and (i) tilting error.

mean squares of errors (RMSE) in all three directions. The case with the smallest value of $P = 5 \times 10^3$ exhibits positioning fluctuations in three DOFs at steady state, as shown in Fig. 7. This is largely due to an inadequate control effort supplied to the VCM to overcome the disturbance of the radial runouts specified in Eq. (18). On the other hand, the case with large value of $P = 5 \times 10^6$ has trouble in stabilizing the tilting motion at steady state, as shown in Fig. 9. This is largely due to the overpowered control effort to the VCM in the tilting direction. In conclusion, the medium value of $P = 5 \times 10^4$ suits best for the controller.

In the next step, the simulations with the parameter values considered in Case 4 in Table 2 are conducted to find suitable value of W for a satisfactory controller performance. In Case 4, with P fixed to the pre-chosen medium value of 5×10^4, W is increased from the value of 10 in Case 1–3 to 1000 for a chance to speed up the convergence near the sliding surface. The corresponding results are shown in Fig. 10. A general comparison between Figs. 8 and 10 renders that an increased W does not significantly shorten response time especially in the transient stage, while brings small levels of fluctuation due to the higher control gain of W near the sliding surface. Note that from Eq.

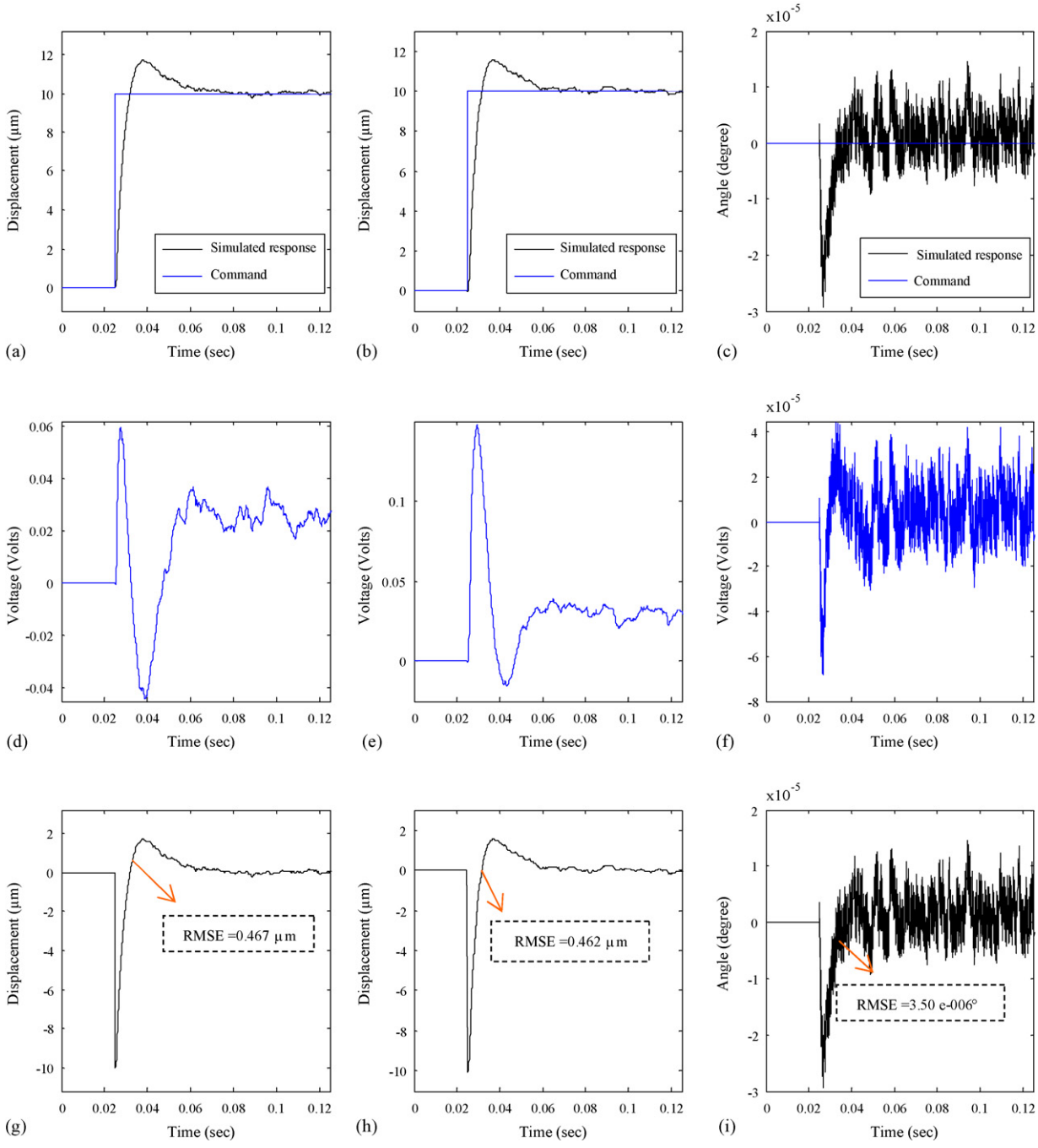

Fig. 9. Simulated step responses, control efforts and errors of the pickup system controlled by the designed SMC in three directions with control parameters of Case 3 given in Table 2. (a) Tracking, (b) focusing, (c) tilting, (d) tracking control effort, (e) focusing control effort, (f) tilting control effort, (g) tracking error, (h) focusing error and (i) tilting error.

(23) it can be perceived that W dictates level of the switching effort near the sliding surface. Therefore, the suitable value of W remains as the pre-chosen 10.

5.2. Choosing observer gains

With the control parameters chosen based on simulations, efforts are paid herein to find suitable observer gains also based on simulations. In the first step, the values of parameters $h_{p,i}$'s and $h_{v,i}$'s, prescribed by Eq. (30), are designated to have $\mathbf{H}_p = \mathbf{diag}[4 \times 10^3,\ 4 \times 10^3,\ 2 \times 10^4]$ and $\mathbf{H}_v = \mathbf{diag}[4 \times 10^6,\ 4 \times 10^6,\ 1 \times 10^8]$ to ensure robust stability of the observer. Second, the small parameter ε is first chosen as $\varepsilon = 0.005$ (as listed in Table 3) for a relative fast convergence on state velocity estimations. The resulted responses are plotted in Fig. 11, where the responses of the controlled system with the feedback velocities estimated from the observer are represented by dot-dashed curves, while those with those actual velocities are represented

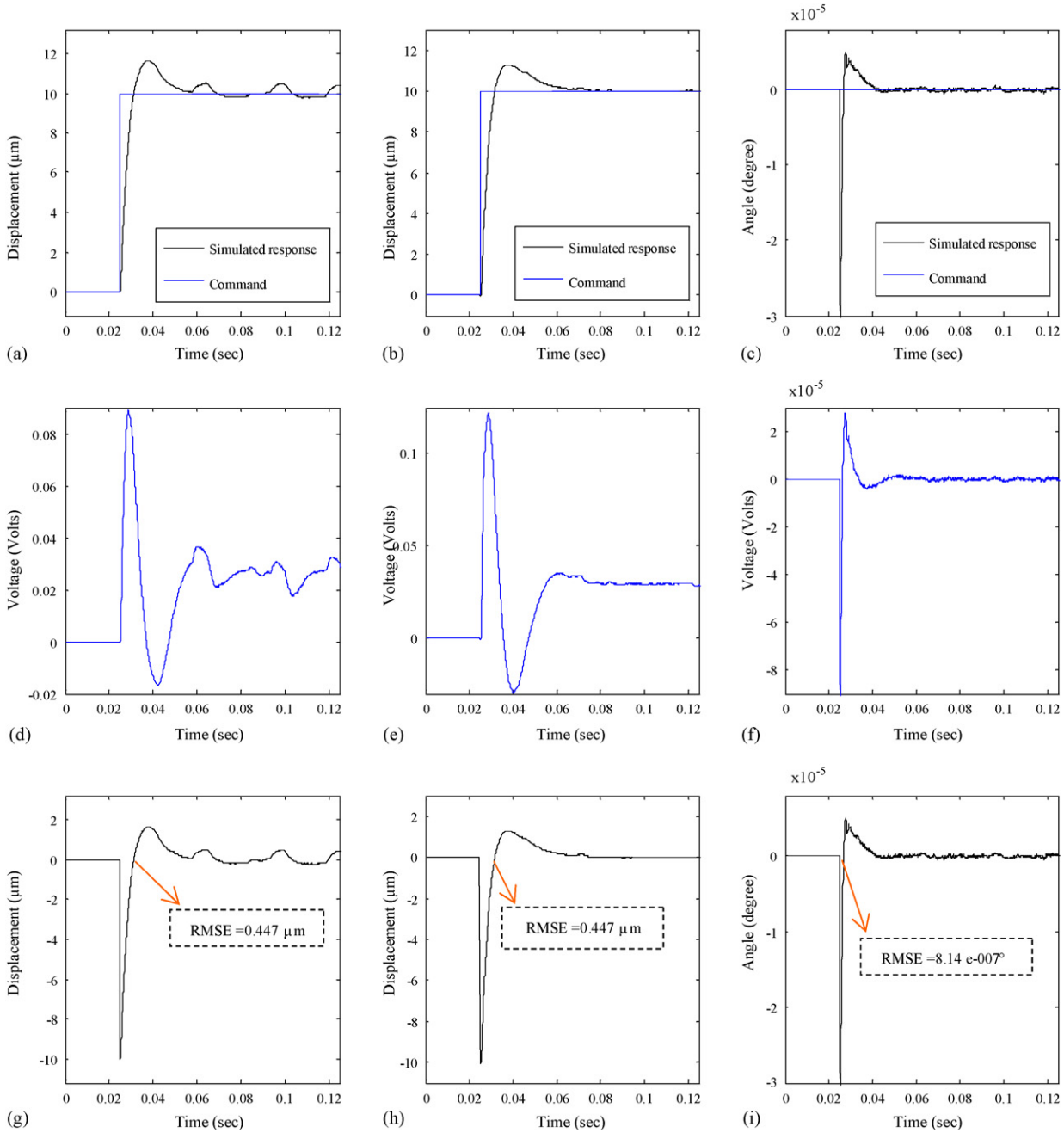

Fig. 10. Simulated step responses, control efforts and errors of the pickup system controlled by the designed SMC in three directions with control parameters of Case 4 given in Table 2. (a) Tracking, (b) focusing, (c) tilting, (d) tracking control effort, (e) focusing control effort, (f) tilting control effort, (g) tracking error, (h) focusing error and (i) tilting error.

by solid curves for comparison. It is seen from the errors in Fig. 11(g–i) that the controller assisted by the high-gain observer achieves precision positionings in the three DOFs of focusing, tracking and tilting. Also, the RMSE values of the controlled system with the observer employed are close to those of actual responses in all 3 DOFs, indicating a satisfactory convergence in velocity estimation by the high-gain observer. ε is next detuned to a even smaller value, the chosen parameter as shown in Table 3, $\varepsilon = 0.0005$, to aim for a better observer convergence. The corresponding simulated responses are plotted in Fig. 12, where it is seen that the controlled responses and errors using the observed velocities are indistinguishable from those of actual counterparts, demonstrating that a smaller $\varepsilon = 0.0005$ is a better choice than $\varepsilon = 0.005$. Note that the previous finding in fact reflects the theoretical core of the high-gain observer. In each

Table 3
Cases for choosing detuning parameter ε

Case no.	P	**Q**	ε
1	5×10^4	10	0.005
2 (also for experiment)	5×10^4	10	0.0005

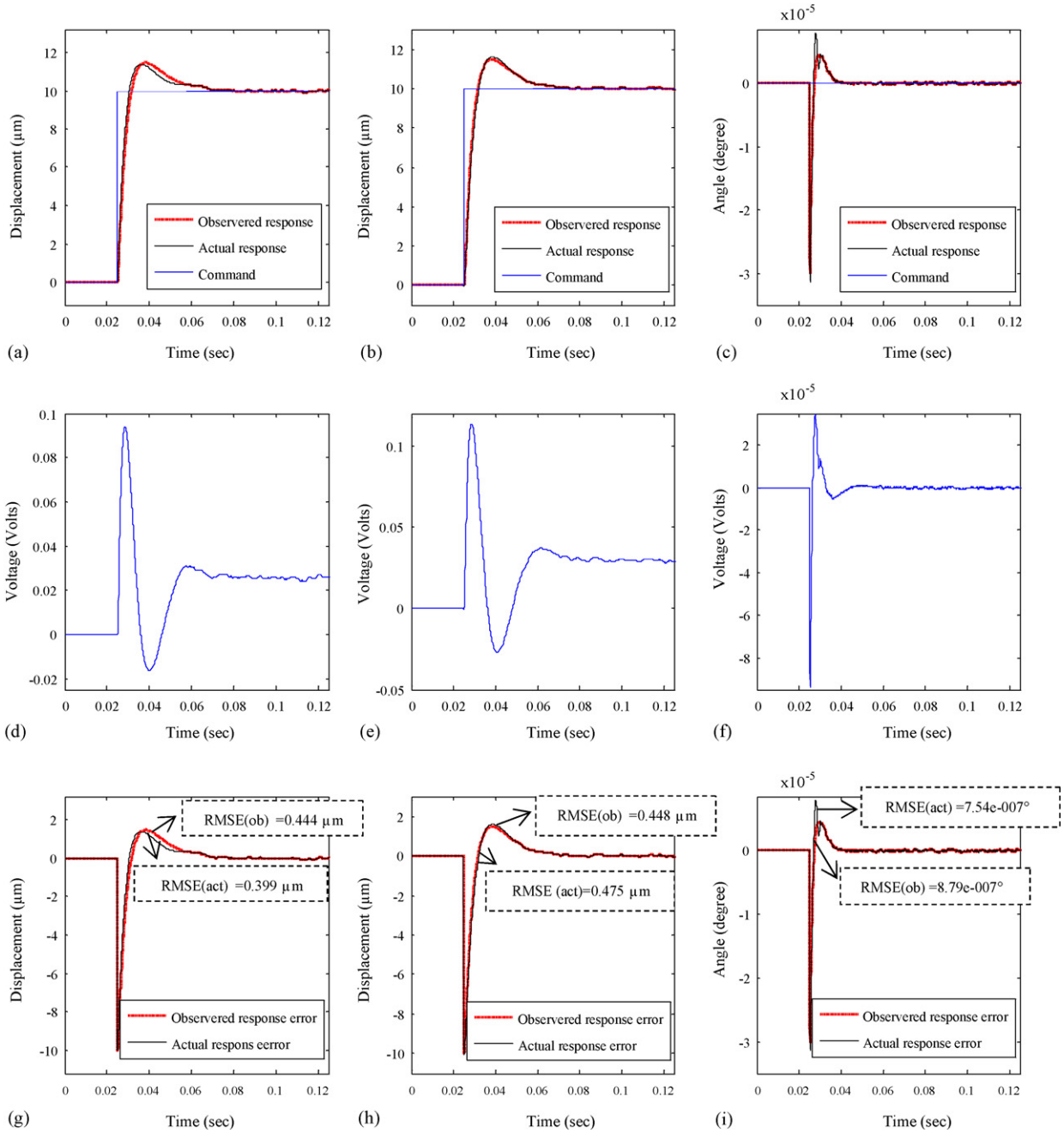

Fig. 11. Simulated step responses, control efforts and errors of the pickup system controlled by the designed SMC assisted by the high-gain observer in three directions. The employed controller and observer parameters are those of Case 1 in Table 3. (a) Tracking, (b) focusing, (c) tilting, (d) tracking control effort, (e) focusing control effort, (f) tilting control effort, (g) tracking error, (h) focusing error and (i) tilting error

design of the observer, one ought to continuously detune the value of ε until the required computation load is bearable for the DSP module utilized.

6. Experimental validation

Experiments are conducted to verify the expected effectiveness of the designed SMC and the high-gain observer with the parameters and gains chosen in Section 5. Fig. 13 illustrates the experimental setup employed, which consists of a laser displacement sensor (MTI 250), two optical fiber displacement sensors (MTI KD-300) and a three-axis pickup provided by the Industrial Technology and Research Institute (ITRI), Taiwan. The implementation of the previously designed controller/observer algorithms are accomplished by a DSP module (dSPACE1103). This DSP accepts the measurements of the bobbin motions from the laser and optical sensors, based on which calculations are conducted following the previously designed controller/observer algorithm to output required control efforts. The output control efforts are further amplified by a custom-

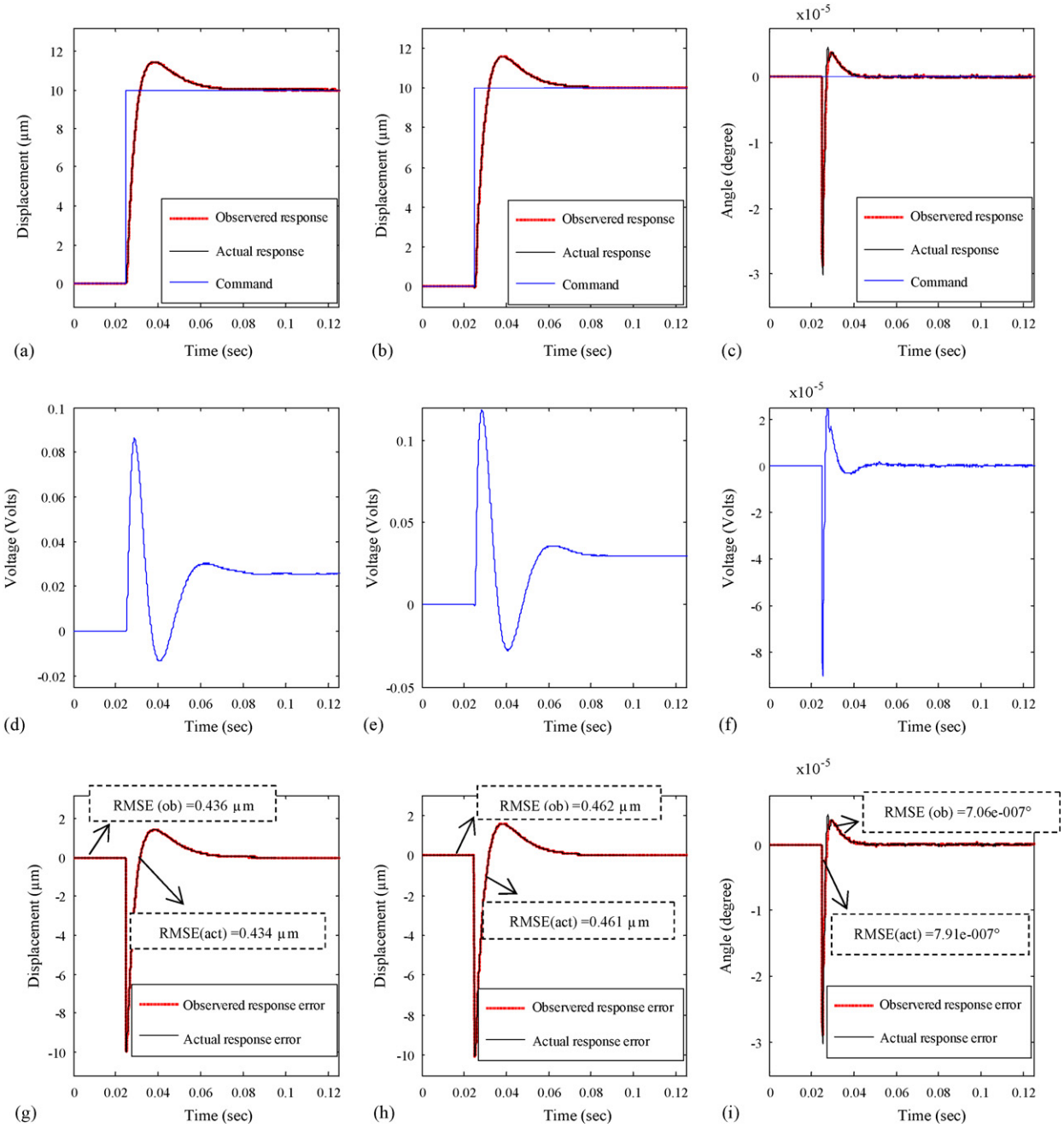

Fig. 12. Simulated step responses, control efforts and errors of the pickup system controlled by the designed SMC assisted by the high-gain observer in three directions. The employed controller and observer parameters are those of Case 2 in Table 3. (a) Tracking, (b) focusing, (c) tilting, (d) tracking control effort, (e) focusing control effort, (f) tilting control effort, (g) tracking error, (h) focusing error and (i) tilting error.

made amplifier circuit featuring chip OP-741 before fed into the pickup for generating bobbin motions. The tracking (horizontal) motions of the bobbin in the pickup are measured directly by the laser displacement sensor, while the focusing (vertical) and tilting motions are calculated from the measurements of the two optical fiber sensors. The focusing motion is obtained by averaging two optical sensor signals, while the tilting motion is by taking the difference between the two sensor signals and then divided by the span between two parallel sensors. Note that the aforementioned averaging and subtraction are conducted by the DSP module. The resolution of the laser displacement is 0.1–0.2 μm, while those of the optical sensors are 0.3–0.5 μm.

It should be also noted at this point that for most of commercial two-axis pickups the detection of bobbin motions is made possible using the differential phase detection (DPD) module that consists of four photo detector patches in a simple configuration as shown in Fig. 14(a). The DPD module outputs the signals that estimate well the bobbin motions in the directions of focusing and tracking. To offer an additional detection of

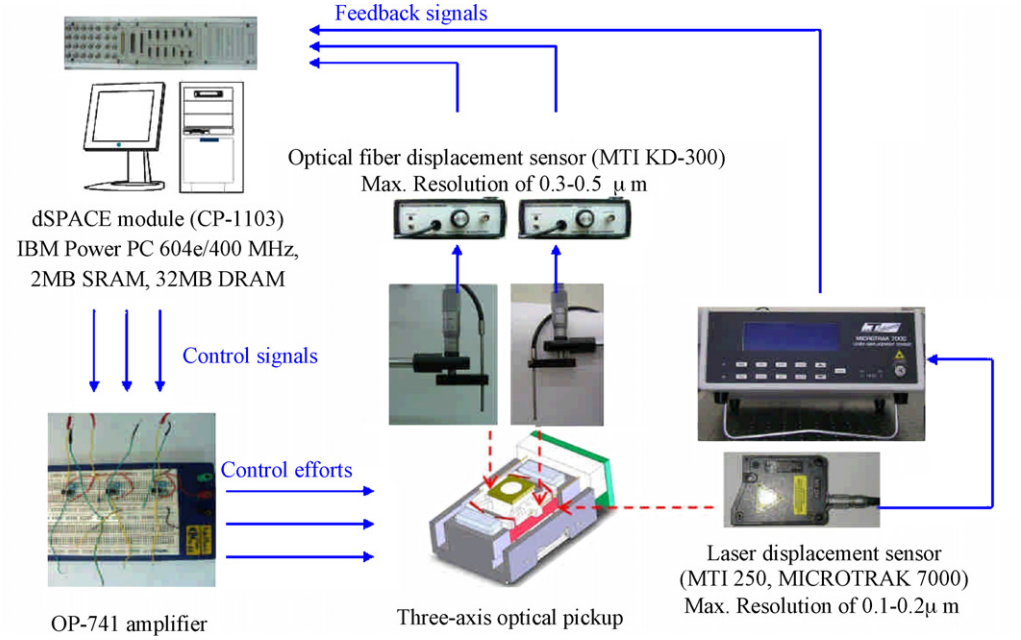

Fig. 13. Schematic diagram of the experimental setup.

the tilting for the three-axis pickups, more receiving patches of photo detectors need to be added to the original DPD module. Fig. 14(b) shows one of new DPD configurations designed by [20], where the four additional patches of A2, B2, C2 and D2 in the middle section make possible the detection of the tilting motion of the bobbin.

Two series of experiments with and without the high-gain observer employed are carried out to validate the expected performance of the proposed controller and observer. Using the control parameters determined previously based on the simulations in Section 5.1, the experiments without the high-gain observer are conducted to verify the expected controller performance in the first series of experimental studies. Fig. 15 plot the experimental responses, control efforts and time histories of positioning errors with theoretical counterparts for comparison, where the experimental precision positioings simultaneously in the directions of focusing, tracking and tilting are clearly achieved, rendering satisfactory steady-state RMSEs of 0.2453 μm, 0.2036 μm and 0.0015°, respectively. Note that the RMSEs obtained herein for tracking and tracking are already close to the resolutions of the used laser and optical sensors, respectively. A general closeness between the theoretical and experimental counterparts is also present despite of little fluctuations involved in the experimental steady-state signals of tracking and focusing. These fluctuations are probably caused by DSP discretization, sensors noises, subsequent digital differentiations and the runouts. Also plotted in these figures are the dashed curves in Fig. 15(c and i) corresponding to the cases without tilting control for comparison. This is made possible in practice by simply switching off the voltage input in the tilting direction. It can be seen from Fig. 15(c and i) that without the tilting control, persistent large non-zero tilting angles are present before and after the control activated, causing a serious difficulty in data-reading by the pickup. Finally, it is seen from the control efforts in Fig. 15(d–f) that larger fluctuations in the control efforts at steady state in Fig. 15(e and f) are present than those in Fig. 15(d). This is due to the fact that the resolution by the laser sensor for the tracking motion is finer than those by the optical sensors responsible for detecting the focusing and tilting motions.

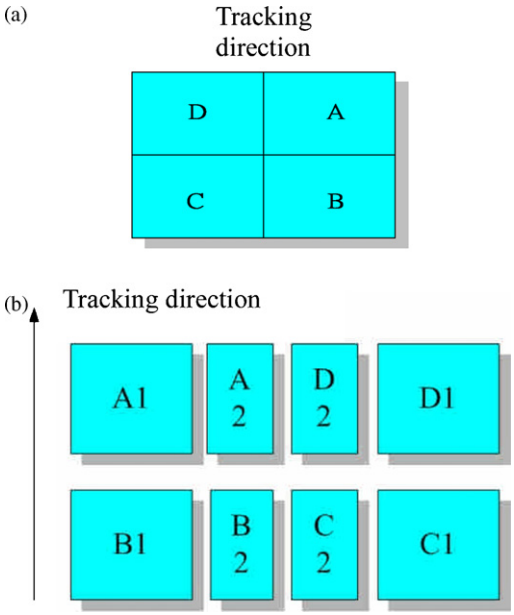

Fig. 14. Photo detector patches of a DPD module.

In the second series of experimental study, the high-gain observer with the gains previously determined in Section 5.2 is augmented into the SMC to verify the expected performance

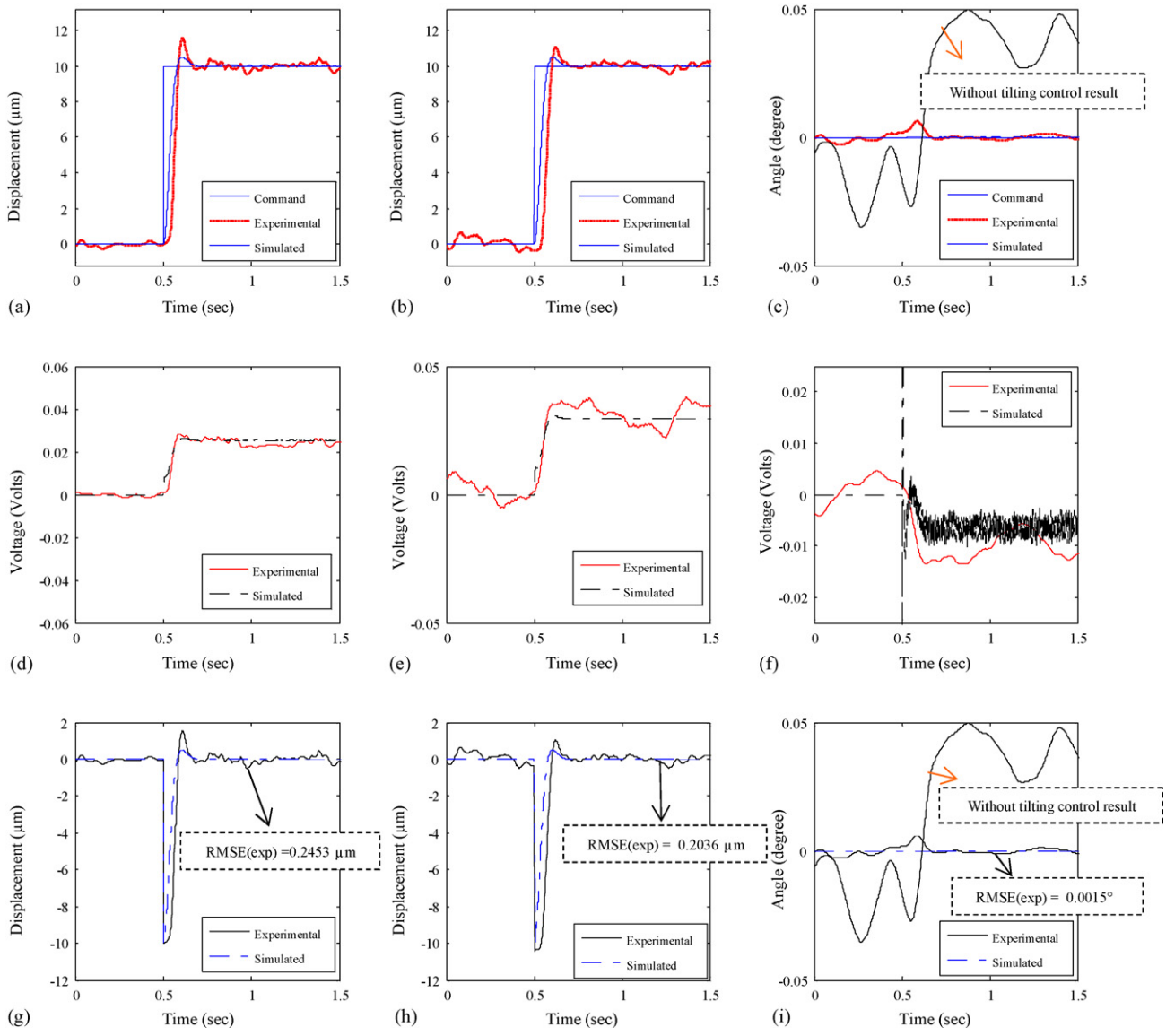

Fig. 15. Experimental and simulated step responses, control efforts and errors of the pickup system controlled by the designed SMC without an observer in three directions. (a) Tracking, (b) focusing, (c) tilting, (d) tracking control effort, (e) focusing control effort, (f) tilting control effort, (g) tracking error, (h) focusing error and (i) tilting error.

predicted theoretically. Fig. 16 plot the experimental responses, control efforts and time histories of errors with the theoretical counterparts for comparison, where it is seen that the synthesized controller and observer are able to perform precision positionings simultaneously in the directions of tracking, focusing and tilting, rendering steady-state RMSEs of 0.1407 μm, 0.1449 μm and 0.0019°, respectively. Note that the RMSEs obtained herein for tracking and tracking are slightly below the resolutions of the used laser and optical sensors, respectively, thanks to the integrations performed by the high-gain observer to reduce noises by the sensors and environment. A general closeness between the simulated curves and experimental counterparts is also present. Comparing the responses in these figures with those counterparts in Fig. 15, where no high-gain observer is applied, it is clear that moderate levels of higher-frequency fluctuations embedded in the error signals in Fig. 15(g–i) are alleviated in the counterpart subfigures, Fig. 16(g–i). This is in fact largely due to the integrations conducted by the high-gain observer, since the observer circumvents the noise induced by DSP digital differentiations. However, this also comes with the cost of longer transient responses, as shown in Fig. 16, for completing the integrations demanded by the observer. Finally, it should also be noted that the large fluctuations in the control efforts in Fig. 16(d and e) prior to the initiation of the step commands are due to the substantial estimation errors of the bobbin velocities induced by the high-gain observer. Based on Eq. (B.5) in Appendix B on the high-gain observer convergence, the aforementioned observer estimation errors can easily be shown inevitable as the positioning errors are close to zeros as before the step commands are initiated.

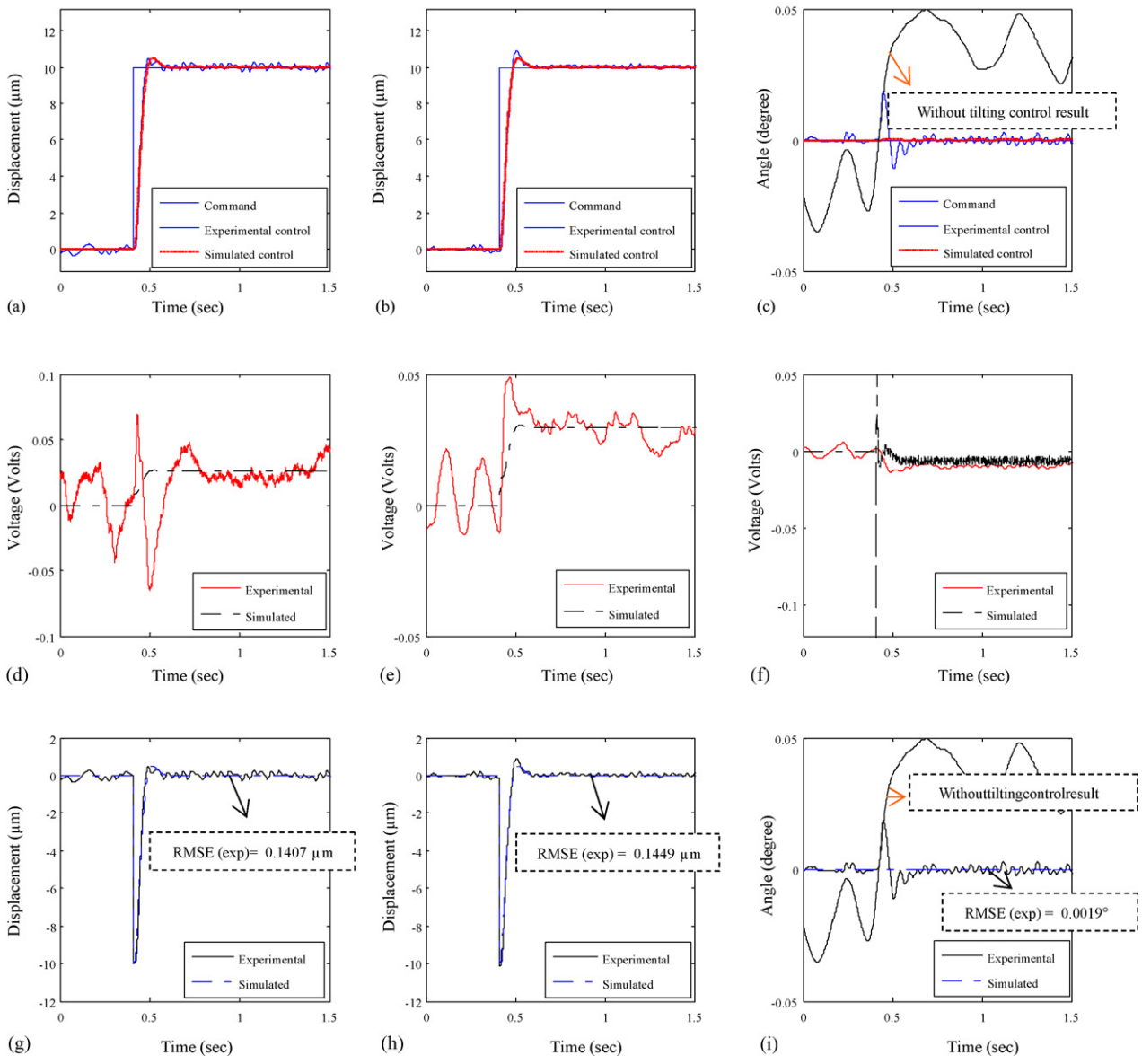

Fig. 16. Experimental and simulated step responses, control efforts and errors of the pickup system controlled by the designed SMC assisted by the high-gain observer in three directions. (a) Tracking control with high-gain observer, (b) focusing control with high-gain observer, (c) tilting angle control with high-gain observer, (d) tracking control effort, (e) focusing control effort, (f) tilting control effort, (g) error, (h) error and (i) error.

7. Conclusions

This study is dedicated to design and experimental validation of a sliding-mode controller equipped with a high-gain observer, which are synthesized for simultaneous precision positionings of a three-axis optical pickup in the directions of focusing, tracking and tilting. Based on the simulated and experimental results, the following conclusions are drawn.

(1) Simulations and experimental studies have demonstrated that the synthesized controller and observer is capable of simultaneously positioning the bobbin in the pickup for precision focusing, tracking and reducing tilting to acceptable, small levels.

(2) The levels of the tilting in the cases without tilting control are found substantially larger than those with the titling control by the designed SMC, showing the importance of employing a three-axis controller and the effectiveness of the accompanied controller/observer algorithm proposed in this study to suppress non-zero tiltings.

(3) The application of the high-gain observer helps greatly for reducing levels of fluctuations in steady-state system responses. These fluctuations are possibly caused by environmental, sensor and digital noises. However, it should also be noted that although fluctuations is reduced, the observer brings the cost of longer transient responses.

Acknowledgments

The authors would like to express special thanks to the Industrial Technology and Research institute (ITRI), Taiwan for their helps with the experimental hardware and setup. The authors are also greatly indebted to the National Science Council of ROC for the financial support through the contacts NSC 93-2212-E-033-001 and NSC 94-2622-E-033-001-CC3, and also to the Center-of-Excellence Program on Membrane Technology, the Ministry of Education, Taiwan, ROC.

Appendix A

The proof to show the satisfaction of the input matching condition is provided herein. Following the procedures in [8,9], the proof starts with re-presenting the system equations in a state-space form as

$$\dot{\mathbf{x}} = \tilde{\mathbf{f}}(\mathbf{x}) + \Delta\tilde{\mathbf{f}}(\mathbf{x}, t) + [\tilde{\mathbf{G}}(\mathbf{x}) + \Delta\tilde{\mathbf{G}}(\mathbf{x}, t)]\mathbf{u}, \qquad \mathbf{y} = \tilde{\mathbf{h}}(\mathbf{x}), \tag{A.1}$$

where

$$\mathbf{x} = [\mathbf{q}\dot{\mathbf{q}}] = [X, Y, \theta, \dot{X}, \dot{Y}, \dot{\theta}]; \quad \tilde{\mathbf{h}}(\mathbf{x}) = \mathbf{q} = [X, Y, \theta];$$

$$\tilde{\mathbf{f}}(\mathbf{x}) = \begin{bmatrix} \hat{\mathbf{I}} \\ -\mathbf{M}^{-1}\mathbf{C}_0\mathbf{q}_2 - \mathbf{M}^{-1}\mathbf{K}_0\mathbf{q}_1 - \mathbf{M}^{-1}\mathbf{D} \end{bmatrix};$$

$$\tilde{\mathbf{G}}(\mathbf{x}) = \begin{bmatrix} \hat{\mathbf{0}} \\ \mathbf{M}^{-1}\bar{\mathbf{T}}_0 \end{bmatrix}; \quad \mathbf{u} = \mathbf{V};$$

$$\hat{\mathbf{I}} = \begin{bmatrix} 0 & 0 & 0 & 1 & 0 & 0 \\ 0 & 0 & 0 & 0 & 1 & 0 \\ 0 & 0 & 0 & 0 & 0 & 1 \end{bmatrix}; \quad \hat{\mathbf{0}} = \begin{bmatrix} 0 & 0 & 0 \\ 0 & 0 & 0 \\ 0 & 0 & 0 \end{bmatrix};$$

and $\{\Delta\tilde{\mathbf{f}}, \Delta\tilde{\mathbf{G}}\}$ are the uncertainties associated with $\{\tilde{\mathbf{f}}, \tilde{\mathbf{G}}\}$, respectively. It can easily be obtained that

$$L_{\tilde{\mathbf{g}}_j}\tilde{h}_i(\mathbf{x}) = 0, \quad \text{for } i, j = 1, 2, 3,$$

$$A \equiv \begin{bmatrix} L_{\tilde{\mathbf{g}}_1}L_{\tilde{\mathbf{f}}}\tilde{h}_1(\mathbf{x}) & L_{\tilde{\mathbf{g}}_2}L_{\tilde{\mathbf{f}}}\tilde{h}_1(\mathbf{x}) & L_{\tilde{\mathbf{g}}_3}L_{\tilde{\mathbf{f}}}\tilde{h}_1(\mathbf{x}) \\ L_{\tilde{\mathbf{g}}_1}L_{\tilde{\mathbf{f}}}\tilde{h}_2(\mathbf{x}) & L_{\tilde{\mathbf{g}}_2}L_{\tilde{\mathbf{f}}}\tilde{h}_2(\mathbf{x}) & L_{\tilde{\mathbf{g}}_3}L_{\tilde{\mathbf{f}}}\tilde{h}_2(\mathbf{x}) \\ L_{\tilde{\mathbf{g}}_1}L_{\tilde{\mathbf{f}}}\tilde{h}_3(\mathbf{x}) & L_{\tilde{\mathbf{g}}_2}L_{\tilde{\mathbf{f}}}\tilde{h}_3(\mathbf{x}) & L_{\tilde{\mathbf{g}}_3}L_{\tilde{\mathbf{f}}}\tilde{h}_3(\mathbf{x}) \end{bmatrix} = \mathbf{M}^{-1}\bar{\mathbf{T}}_0, \tag{A.2}$$

where L denotes Lie Derivative; $\tilde{\mathbf{g}}_j$'s are row vectors of $\tilde{\mathbf{G}}$ while $\tilde{h}_i$'s are components of $\tilde{\mathbf{h}}$. Based on theory of nonlinear control, the content of the computed matrix A in Eq. (A.2) leads to a vector of relative degree of freedom (DOF) of [2, 2, 2] if $\mathbf{M}^{-1}\bar{\mathbf{T}}_0$ is nonsingular. The matrix, $\mathbf{M}^{-1}\bar{\mathbf{T}}_0$, being a function of the pickup tilt angle, can easily be shown nonsingular with the system dynamics considered in this study, due to the fact that the tilting angle is always small. With the relative DOFs obtained, the next step toward the input matching condition is to check if the relative DOFs are unchanged by addition of uncertainties and disturbance, which are prescribed by $\mathbf{C}_\Delta$, $\mathbf{K}_\Delta$ and $\mathbf{T}_\Delta$ in Eq. (17) and $\mathbf{D}$ in Eq. (18), respectively. While in the formulated system Eq. (A.1), they are grouped into $\Delta\tilde{\mathbf{f}}$ and $\Delta\tilde{\mathbf{G}}$. Based on the entrance locations of $\mathbf{C}_\Delta$, $\mathbf{K}_\Delta$, $\mathbf{X}_\Delta$ and $\mathbf{D}$ into $\Delta\tilde{\mathbf{f}}$ and $\Delta\tilde{\mathbf{G}}$, it can easily be deduced that

$$\Delta\tilde{\mathbf{f}} \text{ and } \Delta\tilde{\mathbf{g}}_j \in \mathbf{Ker}[\mathrm{d}\tilde{h}_i], \tag{A.3}$$

since $\mathbf{Ker}[\mathrm{d}\tilde{h}_i] = [\,0 \quad 0 \quad 0 \quad R^3\,]$. With the above condition (A.3) held, the matching condition is henceforth satisfied. Finally note that the system Eq. (18) are in fact ready to be in a normal form with $\mathbf{M}^{-1}$ multiplied at both sides. The relative DOF vector is obviously [2, 2, 2], where each "two" corresponds to one of DOFs of tracking, focusing and tilting. Non-singularity of $\mathbf{M}^{-1}\bar{\mathbf{T}}_0$ and the satisfaction of condition (A.3) mean practically that one could design a control effort $\mathbf{V}$ capable of reaching and suppressing system uncertainties and disturbance for the three-axis pickup considered in this study.

Appendix B

The proof on the estimation convergence of the proposed high-gain observer is provided in this appendix. This proof starts with establishing the equations governing the error dynamics of estimation by the high-gain observer. These equations can be obtained by subtracting Eq. (29) from Eq. (30), yielding

$$\tilde{\mathbf{q}}_1 = \tilde{\mathbf{q}}_2 - \frac{1}{\varepsilon}\mathbf{H}_\mathrm{p}(\tilde{\mathbf{q}}_1),$$

$$\dot{\tilde{\mathbf{q}}}_2 = -\frac{1}{\varepsilon^2}\mathbf{H}_\mathrm{v}(\tilde{\mathbf{q}}_1) + \phi(\mathbf{q}_1, \mathbf{q}_2, \hat{\mathbf{q}}_1, \hat{\mathbf{q}}_2, \mathbf{t}) \tag{B.1}$$

where $\tilde{\mathbf{q}}_i = \mathbf{q}_i - \tilde{\mathbf{q}}_i$, $i = 1, 2$. For further analysis, the following new coordinates and scalings are introduced, i.e.

$$\tilde{\mathbf{z}}_1 = \tilde{\mathbf{q}}_1, \qquad \tilde{\mathbf{z}}_2 = \varepsilon\tilde{\mathbf{q}}_2, \qquad \tilde{\mathbf{z}} = (\tilde{\mathbf{z}}_1^\mathrm{T}, \tilde{\mathbf{z}}_2^\mathrm{T})^\mathrm{T}. \tag{B.2}$$

With the aboves, the error dynamics in Eq. (B.1) can be re-expressed as

$$\varepsilon\dot{\tilde{\mathbf{z}}}_1 = -\mathbf{H}_\mathrm{p}\tilde{\mathbf{z}}_1 + \tilde{\mathbf{z}}_2, \qquad \varepsilon\dot{\tilde{\mathbf{z}}}_2 = -\mathbf{H}_\mathrm{v}\tilde{\mathbf{z}}_1 + \varepsilon^2\phi(\mathbf{q}_1, \mathbf{q}_2, \hat{\mathbf{q}}_1, \hat{\mathbf{q}}_2, \mathbf{t}),$$

or in the matrix form of

$$\varepsilon\dot{\tilde{\mathbf{z}}}_2 = \mathbf{A}_\mathbf{o}(\tilde{\mathbf{z}}) + \varepsilon^2\mathbf{b}\phi(\mathbf{q}_1, \mathbf{q}_2, \hat{\mathbf{q}}_1, \hat{\mathbf{q}}_2, \mathbf{t}), \tag{B.3}$$

where $\tilde{\mathbf{z}} = \begin{bmatrix} \tilde{\mathbf{z}}_1 \\ \tilde{\mathbf{z}}_2 \end{bmatrix}$, $\mathbf{A}_\mathbf{o} = \begin{bmatrix} -\mathbf{H}_\mathrm{p} & \mathbf{I} \\ -\mathbf{H}_\mathrm{v} & 0 \end{bmatrix}$ and $\mathbf{b} = \begin{bmatrix} \mathbf{0} \\ \mathbf{I} \end{bmatrix}$. Since matrices $\mathbf{H}_\mathrm{p}$ and $\mathbf{H}_\mathrm{v}$ have been chosen to place the spectra of $p_i(\lambda)$, $i = 1, \ldots, N$, in the left half plane, there exists a positive definite matrix $\mathbf{P}_\mathbf{o}$ independent of ε to be the solution of the following matrix equation $\mathbf{A}_\mathbf{o}^\mathrm{T}\mathbf{P}_\mathbf{o} + \mathbf{P}_\mathbf{o}\mathbf{A}_\mathbf{o} = -\mathbf{I}$. With the solved $\mathbf{P}_\mathbf{o}$, a new quadratic function defined by $\mathbf{W}(\tilde{\mathbf{z}}) = \tilde{\mathbf{z}}^\mathrm{T}\mathbf{P}_\mathbf{o}\tilde{\mathbf{z}}$ is formed, which can be used to serve as a Lyapunov function candidate for the error dynamics in Eq. (B.3). Computing the derivatives of $\mathbf{W}(\tilde{\mathbf{z}})$ along the solutions of Eq. (B.3) gives

$$\frac{\mathrm{d}\mathbf{W}}{\mathrm{d}t} = \frac{1}{\varepsilon}[\tilde{\mathbf{z}}^\mathrm{T}(\mathbf{A}_\mathbf{o}^\mathrm{T}\mathbf{P}_\mathbf{o} + \mathbf{P}_\mathbf{o}\mathbf{A}_\mathbf{o})\tilde{\mathbf{z}} + 2\varepsilon^2\phi^\mathrm{T}\mathbf{b}^\mathrm{T}\mathbf{P}_\mathbf{o}\tilde{\mathbf{z}}]$$

$$= -\frac{1}{\varepsilon}\tilde{\mathbf{z}}^\mathrm{T}\tilde{\mathbf{z}} + 2\varepsilon\phi^\mathrm{T}\mathbf{b}^\mathrm{T}\mathbf{P}_\mathbf{o}\tilde{\mathbf{z}}. \tag{B.4}$$

Eq. (B.4) further gives

$$\frac{\mathrm{d}\mathbf{W}}{\mathrm{d}t} \le \frac{1}{\varepsilon}\|\tilde{\mathbf{z}}\|^2 + 2\varepsilon\,\|\mathbf{P}_\mathbf{o}\mathbf{b}\phi\|\,\|\tilde{\mathbf{z}}\|.$$

Based on the above inequality, the convergence of the designed high-gain observer can be ensured by detuning the parameter ε small enough to satisfy

$$\varepsilon^2 < \frac{\|\tilde{\mathbf{z}}\|}{2\left\|\mathbf{P}_0\mathbf{b}\phi(\mathbf{q}_1, \mathbf{q}_2, \hat{\mathbf{q}}_1, \hat{\mathbf{q}}_2, t)\right\|}. \tag{B.5}$$

It should be noted at this point that the controlled system always renders a finite quantity of the right hand side in inequality (B.5) before reaching the infinite time. Therefore, there must exist a small value of ε for observer convergence before all positioning errors are very close to zeros. In the actual process of determining ε, one can detune ε from a moderate small value with the assistance from simulations until the observer reaches its required convergence speed for control use. The required convergence speeds of the observation errors $\{\tilde{\mathbf{q}}_1, \tilde{\mathbf{q}}_2\}$ are usually set much faster than the targeted convergence speeds of states $\{\mathbf{q}_1, \mathbf{q}_2\}$, in order to ensure the overall convergence of the control errors.

References

[1] M. Nagasato, I. Hoshino, Development of two-Axis actuator with small tilt angles for one-piece optical head, Jpn. J. Appl. Phys., Part 1 35 (1996) 392–397.

[2] I.H. Choi, S.N. Hong, M.S. Suh, D.H. Son, Y.L. Kim, K.W. Park, J.Y. Kim, 3-Axis actuator in slim optical pick-up for disc tilt compensation, in: Proceedings of Optical Storage Topical Meeting, 2001, pp. 178–180.

[3] J.Y. Kang, M.G. Yoon, Robust control of an active tilting actuator for high-density optical disk, in: Proceedings of the American Control Conference, 1998, pp. 861–865.

[4] G.V. Rosmalen, A floating lens actuator, in: Proceedings of International Symposium on Optical Memory, 1987.

[5] S. Yamada, S. Nishiwaki, A. Nakamura, T. Ishida, H. Yamaguchi, Track center servo and radial tilt servo system for digital versatile rewritable disc (DVD-RAM), Jpn. J. Appl. Phys., Part 1 2B (2000) 867–870.

[6] P.C.P. Chao, J.S. Huang, C.L. Lai, Intelligent control design for a three-DOF four-wire type optical pickup, Sens. Actuator A Phys. 117 (1) (2005) 28–40.

[7] J.J. Slotine, W. Li, Applied Nonlinear Control, Prentice-Hall, New Jersey, USA, 1991.

[8] V.I. Utkin, Sliding Modes and their Applications in Variable Structure Systems, Moscow, 1978.

[9] H. Elmali, N. Olgac, Robust output tracking control of nonlinear MIMO systems via sliding mode technique, Automatica 28 (1) (1992) 145–151.

[10] G. Besancon, Further results on high gain observes for nonlinear systems, in: Proceedings of the 38th Conference on Decision & Control, 1999, pp. 2904–2909.

[11] A. Dabroom, H.K. Khalil, in: Proceedings of the 36th Conference on Decision & Control, Numerical differentiation using high-gain observers (1997) 4790–4795.

[12] J.A. Heredia, W. Yu, A high-gain observer-based PD control for robot manipulator, in: Proceedings of the American Control Conference, 2000, pp. 2518–2522.

[13] A. Isidori, Nonlinear Control Systems, third ed., Springer, Berlin, New York, USA, 1995.

[14] H.K. Khalil, Nonlinear Systems, third ed., Prentice Hall, Upper Saddle River, NJ, USA, 2002.

[15] S. Nicosia, A. Tornambe, P. Valigi, Experimental results in state estimation of industrial robots, in: Proceedings of the 29th Conference on Decision and Control, 1990, pp. 360–365.

[16] E.S. Shin, K.W. Lee, Robust output feedback control of robot manipulators using high-gain observer, in: Proceedings of the International Conference on Control Applications, 1999, pp. 881–886.

[17] L. Meirovitch, Analytical Methods in Vibrations, Macmillan, London, UK, 1967.

[18] K. Milton, Basic Electricity: Theory & Practice, McGraw-Hill, New York, USA, 1973.

[19] K. Zhou, J.C. Doyle, Essentials of Robust Control, Prentice-Hall, New Jersey, USA, 1998.

[20] T.Y. Doh, B.I. Ma, B.H. Choi, I.S. Park, C.S. Chung, Y.H. Lee, S.J. Kim, D.H. Shin, Radial tilt detection using one beam and its compensation in a high-density only memory, Jpn. J. Appl. Phys., Part 1 35 (2001) 1680–1683.

Biographies

Paul C.-P. Chao received his BS in 1989 from National Cheng-Kung University, Tainan, Taiwan. He received MS and PhD degree from Michigan State University, USA, respectively, in 1993 and 1997. After graduation, he worked for the CAE department of Chrysler Corp. in Auburn Hill, Detroit, USA for 2 years. Then he became faculty member of mechanical engineering department at Chung Yuan University, Chung-Li, Taiwan. He published a series of papers on centrifugal pendulum vibration absorbers (CPVAs) and the automatic balancer system (ABS). Prof. Chao was the recipient of the 1999 Arch T. Colwell Merit Best Paper Award from Society of Automotive Engineering, Detroit, USA; the 2004 Long-Wen Tsai Best Paper Award from National Society of Machine Theory and Mechanism, Taiwan; the 2005 Best Paper Award from National Society of Engineers, Taiwan; and the 2002/2003/2004 CYCU Innovative Research Award. He currently serves as Associate Editor of Journal of Advanced Engineering, CYCU, 2005.

In recent years, his research interests focus on micro-mechatronics, optical drives, control technology, micro-sensors and actuators.

Chien-Yu Shen received BSE and MS degrees in civil engineering and mechanical engineering from Chung Yuan Christian University of Taiwan in 2002 and 2004, respectively. He is pursuing a doctor's degree in mechanical engineering at Chung Yuan Christian University, Taiwan. His research interests are advanced control theory, design and implementation of controllers, especially with efforts dedicated to precision positioning of optical pickups.